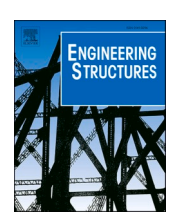
\$ SUPER

Contents lists available at ScienceDirect

Engineering Structures

journal homepage: www.elsevier.com/locate/engstruct





Predicting single freestanding transmission tower time history response during complex wind input through a convolutional neural network based surrogate model

Jiayue Xue, Zhongming Xiang, Ge Ou

Department of Civil and Environmental Engineering, University of Utah, Salt Lake City, UT 84112, United States

ARTICLE INFO

Keywords: Dynamic analysis Time history prediction Surrogate model Complex wind input Transmission tower

ABSTRACT

As the steel towers in the power system are vulnerable to intensive wind loads, it is essential to understand their dynamics response to estimate its potential failure. Conventional structural analysis methods like the finite element analysis or the field test are either computational heavy or cost expensive. Thus, this paper proposes a machine learning approach based on convolutional neural network (CNN) to predict the time history response of the transmission tower during the complex wind input. By preprocessing the time history of wind load and the tower's dynamic response, a well-developed CNN can capture the time and spatial correlation of the wind load successfully and provide high accuracy results. CNN configuration, window size selection, and training data scale are carefully discussed to optimize the CNN design to maximize the prediction accuracy as well as minimize its computational time. Finally, to evaluate the performance of the surrogate model, the accuracy of the optimal CNN is tested in predicting the time history response of the transmission tower under 15 m/s to 70 m/s wind speed. The effectiveness of the CNN surrogate model is validated through a fragility model development, and its robustness is investigated using two wind inputs generated from a random wind profile and a random wind spectrum.

1. Introduction

The transmission tower, a vital support structure of the power system, is vulnerable to extreme wind loads. Like other lifeline systems, the damage of a power system due to transmission tower collapse can lead to a power outage for millions of people in a vast region. Hurricane Harvey, in 2017, affected 2.02 million people with over 850 transmission structures down or damaged [1]; Hurricane Michael, in 2018, caused widespread power outages in Florida, Alabama, and Georgia [2]. To reduce the hurricane-induced damage to the power system, it is essential to accurately capture the performance of a transmission tower during dynamic wind.

Conventional structural analysis of a transmission tower's dynamic response during wind loading includes field and laboratory testing, static and dynamic modeling through finite element analysis, and reliability modeling. The field and laboratory testing provide the most trustworthy result to demonstrate the static or dynamic response of a transmission tower [3-6]. The field test of the transmission tower verifies the novel design of transmission tower [7]; illustrates the load-

bearing capacity and failure mechanism of a transmission tower due to various loading [8]; present the large deformation analysis [9], etc. Wind tunnel tests of the transmission tower usually employ the aeroelastic models to evaluate the transmission tower-line system's actual behaviors [10-12]. The obtained knowledge from the field and laboratory test is further utilized in structural modeling using finite element analysis. Finite element models are used to develop a static and dynamic response of the transmission tower or tower-cable system. For static analysis, the nonlinearity analysis is commonly implemented to estimate the transmission tower's performance under different load patterns based on different national and international design codes [13] or to evaluate its failure by buckling analysis [14-16] with push over loading protocols. For dynamic analysis, the deterministic time history analysis is conducted with complex wind input simulated with theoretical wind characteristics and aeroelastic loading parameters obtained from wind tunnel test [17-20]. With the combination of 1) a static analysis which develops the failure criterion of the transmission tower, 2) a deterministic time history analysis of transmission tower considers different wind loading conditions, and 3) a Monte Carlo simulation process realizes

E-mail addresses: jiayue.xue@utah.edu (J. Xue), zhongming.xiang@utah.edu (Z. Xiang), ge.ou@utah.edu (G. Ou).

^{*} Corresponding author.

system aleatoric uncertainties, the reliability model (often the fragility curve or fragility surface) of the transmission tower can be developed [21-23]. Although there are different approaches to obtain the structural response of the transmission tower, it is either computationally expensive or cost expensive.

To allow time-efficient evaluation of structural dynamic response, researchers have investigated different methods to develop surrogate models. Existing surrogate models are majorly developed for structural static analysis problems [24-26], extreme value problems [27], and binary classification problems (predicts failure or non-failure condition) [28-30]. VanLuchene and Sun [31] are the early researchers who developed the surrogate models of a concrete beam and rectangular plate to predict the maximum moment by neural network. With the rapid advances in computer science, more promising surrogate models that predict the structural performance have been developed recently. For the structural static analysis problem, Mukherjee and Biswas [32] successfully obtained the reliable concrete response under high temperature and pressure by artificial neural networks (ANN) without measuring a large number of parameters. In a more recent study, Mohammadhassnai et al. [33] compared ANN with linear regression (LR) to devise a surrogate model of the deep concrete beam for predicting the strain in the tie section. The extreme value problem also stimulates many researchers to develop surrogate models to evaluate the limit state of a structure. Ceylan et al. [34] applied ANN to develop the surrogate model of the pavement to obtain its critical responses and deflection profiles. Oh et al. [35] implemented the time and frequency domain of wind and the corresponding displacement as input to develop the surrogate model by convolutional neural network (CNN) and predict the maximum and minimum strain. The extreme value problem leads to a more critical and straightforward problem, the binary classification problem. Different approaches are brought into this area: Su et al. [36] combined Gaussian Process Regression and Monte Carlo Simulation to develop a surrogate model for the complex structure; Zhao [37] and Sainct et al. [38] employed the active learning like support vector machines (SVM) to conduct structural reliability analysis; Afshari and Liang [39] evaluated the reliability of a cantilever beam by a time-variant degradation model using a Naïve Bayesian Classifier. Perera et al. [40] developed a roaming damage method to detect the damage location by neural network directly and flexibly.

However, there are only a few studies focused on developing a surrogate model to predict structural dynamic time history. To date, the structural dynamic time-history response prediction concentrates mainly on the seismic response prediction [41,42]. The state-of-the-art research employed the deep learning method, the long short-term memory to predict the seismic response [43] while compared to seismic loading, wind loading is more complicated because of its time and spatial correlation. The existing solution to the complex wind load input is to extract the features of the wind load, like the wind-induced acceleration [44] and the coordinate of wind pressure [45], as the input to predict the time series of pressure during wind load.

In wind-induced structural response analysis, the wind load is considered a dynamic time history that can be decoupled into the mean wind and fluctuation wind components. The mean wind speed varies along with the height following a wind profile [46,47], and the fluctuation wind can be statistically presented by a stochastic process generated with a power spectrum in the frequency domain [48]. The spatial correlation of the fluctuating wind also resides and is exhibited by a cross-spectral density spectrum. Therefore, wind loading is a stochastic process which shows strong time and spatial-correlation even with a determined wind profile and spectrum. In addition to the genuine stochasticity in the wind input, other uncertainties are inevitable. As compared to a determined profile, wind profiles have disunited patterns [49,50] due to the spatially dispersed topographies [49]. The frequency content of the wind spectrum describes the turbulent motion in the air, is caused by complex atmospheric phenomenon and conditions [51,52]. Many wind spectra are proposed, which can be classified as height independent (i.e., Davenport's model, and Harris's spectrum) and height dependent (i.e., Von Karman's spectrum, Kaimal's spectrum, and Simiu's spectrum.) based on curve fitting results for different records of intensive wind [48,53,54]. Capturing these uncertainties is a vital problem to obtain the structural response during wind loads. The surrogate model to represent structural response under wind loading should reflect these uncertainties.

In this study, if the time and spatial variant wind speeds are preprocessed into a horizontal and vertical direction of an image respectively, it is possible to employ the powerful image process network, CNN, to interpret the time and spatial dependent wind loading input, as well as its impact to civil infrastructure. As a variety of multiplayer perception, CNN was first proposed by Lecun et al. [55] to recognize the documents with image format. After the modification conducted by Krizhevsky et al. [56], researchers have proposed several versions of CNN that showed promising performance in object recognition from massive images [57-60]. Compared with other machine learning methods (i.e., multilayer perception, support vector machine), CNN has a significant superiority that omits the complicated stage of feature extraction, which has attracted much attention from the researchers in structural simulation [61,62]. Structural damage detection [63-66] and crack detection [67-70] are two primary applications in structural analysis.

In this paper, a novel approach is developed to predict the full-time history response of a transmission tower with dynamic wind load using CNN. A hypothesis is proposed that CNN based learning algorithm can be utilized to capture the temporal and spatial correlation, and the wind profile and spectrum uncertainties of wind loading and its impact on the structural dynamic response. Such surrogate model should be computational effective as compared to deterministic finite element model, at the same time be adaptive to the wind loading characteristics as compared to probabilistic approach such as fragility models. To validate this hypothesis, a CNN-based dynamic response prediction of the transmission tower during wind load approach is proposed, as demonstrated in Fig. 1. A set of training and testing data is generated by obtaining the dynamic response of the transmission tower with wind simulation and numerical model development. These data are preprocessed and then used to train the network. Finally, the trained CNN is employed to predict the dynamic response of a transmission tower during wind load and further develop a reliability model (fragility model) during complex wind conditions.

The rest of this paper is organized as follows: Section 2 introduces the characteristics and simulation of the wind load input, the numerical model of the transmission tower, and its dynamic response. Section 3 details the methodology by introducing the architecture of CNN and its application of an infrastructure system. Section 4 conducts a parametric study to compare the impact of CNN configuration, window size selection, and training data scales on the prediction performance. Section 5 employs the developed CNN structure and proper coefficients to a broad wind speed range, its effectiveness is demonstrated through the development of the fragility model of the tower, and its robustness is tested using a random profile and spectrum. Section 6 summarizes the conclusions of this proposed method and proposes future work.

2. Wind load model and numerical model

To implement the proposed convolutional neural network (CNN) for the wind-induced response of the transmission tower, the dynamic load of the wind speed is simulated first, and a numerical model of the transmission tower is developed after that, which is shown in Fig. 2. In this section, the characteristics and simulation of the dynamic wind input are further discussed. The numerical information of the transmission tower is provided after that. Finally, the time history response of the transmission tower during complex wind input is presented. This numerical simulation process generates the dataset for further CNN training and testing.

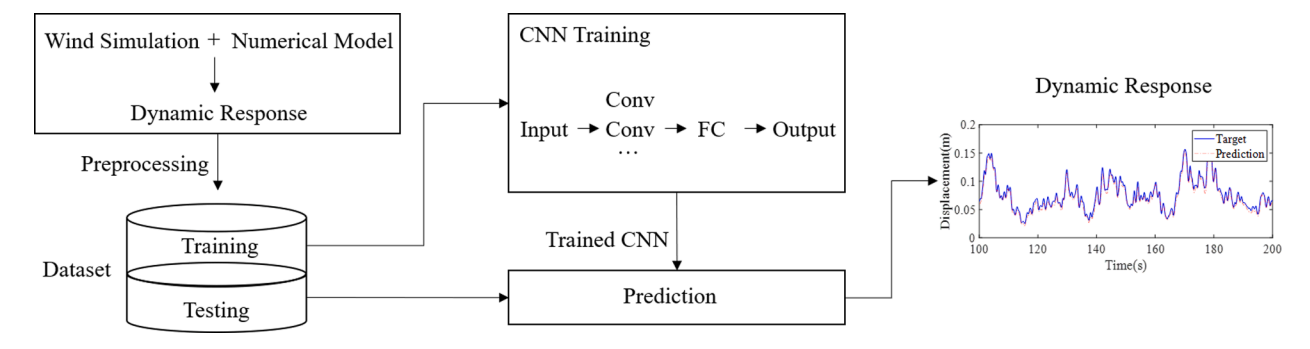


Fig. 1. Flow Chart of A CNN-based Dynamic Response Prediction of Transmission Tower.

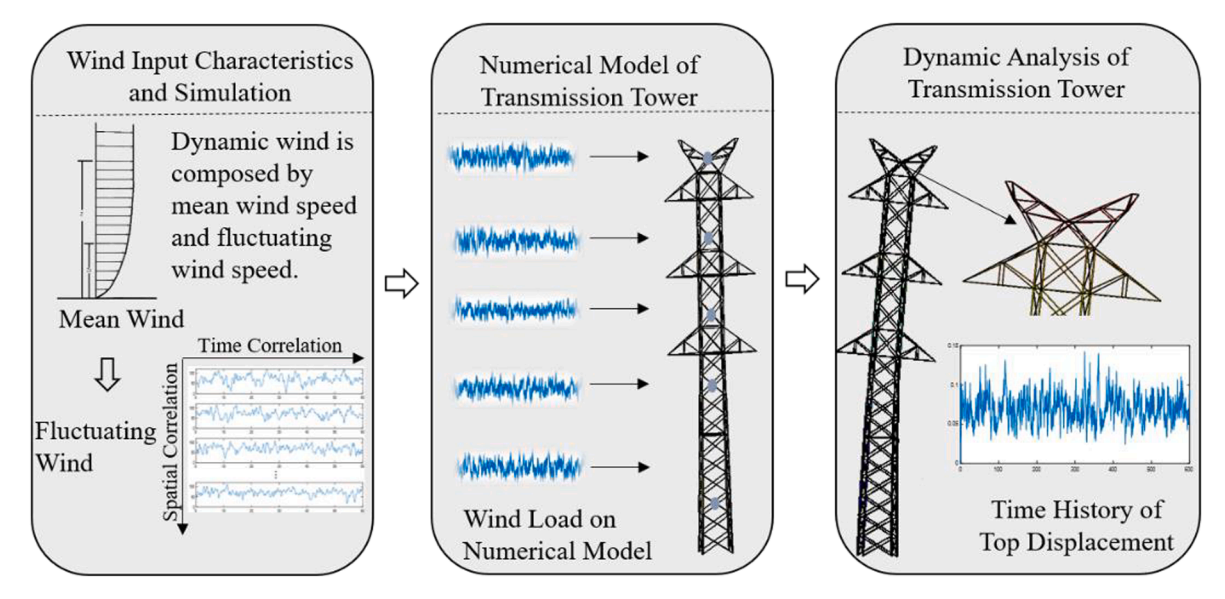


Fig. 2. Numerical Simulation Process for Data Generation.

2.1. Wind input characteristics and simulation

Compared with some simplified work, which adopts the seismic ground acceleration as the single input, wind load is more complicated because of its time and spatial correlation. The stochastic wind simulation is composed of the mean and fluctuating wind as Eq. (1). The mean wind profile changes over height by a power law based on ASCE 7-98 in Eq. (2) [84].

$$V(t) = \overline{V} + V_j \tag{1}$$

$$\frac{\overline{V}}{\overline{V}_{10}} = \left(\frac{z}{z_{10}}\right)^{\alpha} \tag{2}$$

where V(t) is the stochastic wind; \overline{V} is the mean wind speed at different heights; V_j is the fluctuating wind; \overline{V}_{10} is the reference mean wind speed at 10 m height; z is the mean wind speed height; and z_{10} is the reference height, 10 m; α is the ground roughness coefficient.

The characteristics of fluctuating wind include its time correlation and spatial correlation. The time correlation of the fluctuating wind is realized by a Gaussian stationary random process. For an n-dimensional zero-mean stationary Gaussian random process $\nu_j(t)(j=1,2,\hat{A}\cdot\hat{A}\cdot\hat{A}\cdot,nt)$, the spectral density matrix is shown in Eq. (3).

$$S(\omega) = \begin{bmatrix} S_{11}(\omega)S_{12}(\omega)\hat{\mathbf{A}}\cdot\hat{\mathbf{A}}\cdot\hat{\mathbf{A}}\cdot S_{1n}(\omega) \\ S_{21}(\omega)S_{22}(\omega)\hat{\mathbf{A}}\cdot\hat{\mathbf{A}}\cdot\hat{\mathbf{A}}\cdot S_{2n}(\omega) \\ \hat{\mathbf{A}}\cdot\hat{\mathbf{A}}\cdot\hat{\mathbf{A}}\cdot \\ S_{n11}(\omega)S_{n2}(\omega)\hat{\mathbf{A}}\cdot\hat{\mathbf{A}}\cdot\hat{\mathbf{A}}\cdot S_{nnt}(\omega) \end{bmatrix}$$
(3)

To obtain the power spectrum of the fluctuating wind, the auto power spectrum of fluctuating wind $S_{\nu}(f)$ at frequency f is defined by Davenport spectrum [72], which is shown as follows,

$$S_{v}(f) = 4\kappa \overline{V_{10}}^{2} \frac{x^{2}}{f(1+x^{2})^{4/3}} x = \frac{1200f}{\overline{V_{10}}}$$
(4)

where κ is the surface drag coefficient.

The spatial correlation of the fluctuating wind is exhibited by its cross-spectral density spectrum $S_{ij}(r,f)$. It is calculated by each panel's auto power spectrum from Eq. (4).

$$S_{ij}(r,f) = \sqrt{S_{ii}(z_i,f)S_{jj}(z_j,f)}Coh(r,f), i \neq j$$
(5)

$$Coh(r,f) = exp(\frac{-2f\sqrt{C_{y}^{2}(y_{i}-y_{j})^{2} + C_{z}^{2}(z_{i}-z_{j})^{2}}}{\overline{V}(z_{i}) + \overline{V}(z_{j})})$$
 (6)

where $C_y = 8$ and $C_Z = 7$ are chosen usually. y_i , y_j , z_i and z_j are the spatial coordinate. It is decomposed by Cholesky decomposition.

$$S(\omega) = H(\omega)H^*(\omega)^T \tag{7}$$

$$H(\omega) = \begin{bmatrix} H_{11}(\omega)0\hat{\mathbf{A}}\cdot\hat{\mathbf{A}}\cdot\hat{\mathbf{A}}\cdot\mathbf{0} \\ H_{21}(\omega)H_{22}(\omega)\hat{\mathbf{A}}\cdot\hat{\mathbf{A}}\cdot\hat{\mathbf{A}}\cdot\hat{\mathbf{A}} \\ \hat{\mathbf{A}}\cdot\hat{\mathbf{A}}\cdot\hat{\mathbf{A}}\cdot\hat{\mathbf{A}}\cdot\hat{\mathbf{A}}\cdot\hat{\mathbf{A}}\cdot\hat{\mathbf{A}}\cdot\hat{\mathbf{A}}\cdot\hat{\mathbf{A}}\cdot\hat{\mathbf{A}} \\ H_{n11}(\omega)H_{nn2}(\omega)\hat{\mathbf{A}}\cdot\hat{\mathbf{A}}\cdot\hat{\mathbf{A}}\cdot\hat{\mathbf{A}}\cdot\hat{\mathbf{A}}H_{nnt}(\omega) \end{bmatrix}$$
(8)

Fluctuating wind $v_j(y_j, z_{j,t})$ is calculated in (9)-(10).

$$v_{j}(y_{j}, z_{j,t}) = \sqrt{2(\Delta \omega)} \sum_{m=1}^{j} \sum_{l=1}^{N} |H_{jm}(\omega_{ml})| cos(\omega_{ml}t - \theta_{jm}(\omega_{ml}) + \varphi_{ml}) j$$

$$= 1, 2, \hat{A} \cdot \hat{A} \cdot \hat{A} \cdot nt$$
(9)

$$\omega_l = (l-1)\Delta\omega + \frac{m}{N}\Delta\omega, l = 1, 2, \hat{\mathbf{A}}\cdot\hat{\mathbf{A}}\cdot\hat{\mathbf{A}}\cdot, N$$
(10)

where $\mathrm{H}(\omega)$ is the Cholesky decomposition matrix; $\Delta\omega$ is frequency increment; N is a positive large integer. Fig. 3 illustrates the dynamic wind on the top of the transmission tower and a comparison between the simulated spectrum and the Davenport spectrum.

Based on the simulated wind speed, the dynamic wind load added on each panel of the transmission tower is calculated as (11).

$$F = 0.5\rho V(t)^2 C_f A_m \tag{11}$$

where ρ is the air density; V(t) is wind time history, obtained from Eqs. (1)–(10); C_f is the drag coefficient; A_m is the projected area.

2.2. Numerical model of transmission tower

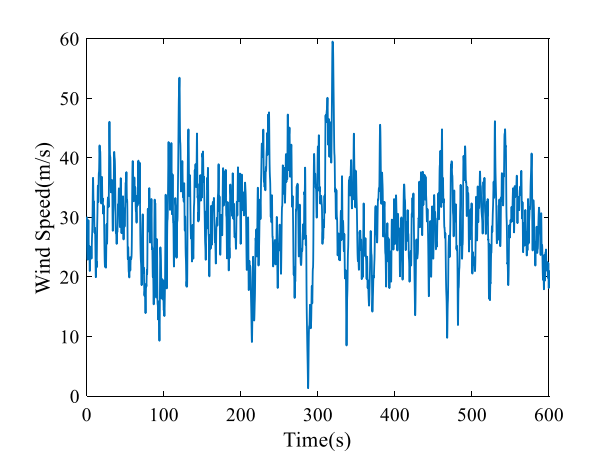
The transmission tower shown in Fig. 2 is employed in this paper to validate the efficiency of CNN. It is a suspension tower initially described by Tort et al. [73] and redesigned for the hurricane zone based on ASCE Manual 74 Guidelines for Electrical Transmission Line Structural Loading [71]. The height of the transmission tower is 31.5 m. All members are steel-made (ASTM A36), L-shape cross-sections. The finite element model of the transmission tower is developed by ANSYS, a commercial finite element software.

2.3. Dynamic response of transmission tower during wind load

By adding a set of wind loads on different panels of the transmission tower, the dynamic response of the transmission tower during wind load is obtained as Fig. 4. Usually, the top displacement is selected as an index to evaluate the failure or collapse of the transmission tower [74].

3. Methodology

As noted above, the inducement from the dynamic wind speed can result in the displacement of the transmission tower. Despite the time and spatial dependence, the inputs (wind speed) of the inducement are the two-dimension (2D) shapes. As shown in Fig. 5, if the wind speeds $p_1, p_2, p_3 \cdots p_n$ are put together, the two directions of the matrix denote



(a) Wind Speed at Top of First Tower

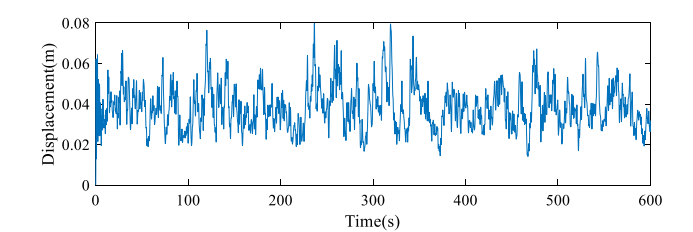


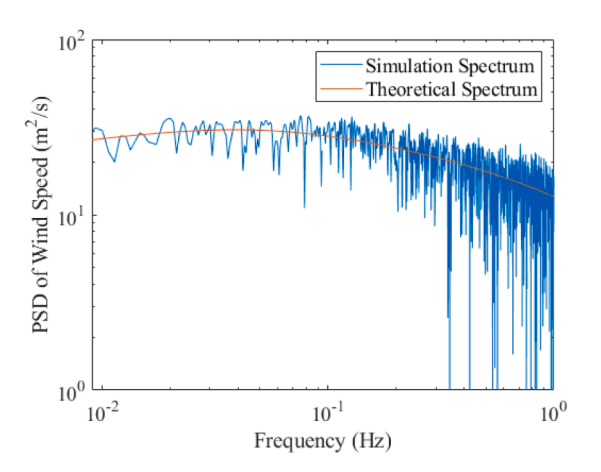
Fig. 4. Top Displacement of Transmission Tower during Wind Load.

the time and spatial correlation horizontally and vertically. Each wind speed at each time step can be converted to a pixel intensity of the single channel image. When all the wind speeds at each time step and location are combined together, this data format is similar to the standard input of the convolutional neural network (CNN), which is the 2D image. Hence, this phenomenon provides an intuitive approach of using CNN to replace the traditional simulation with the finite element model. In this paper, CNN is introduced to automatically learn features from the wind speed and then predict the dynamic response of the transmission tower. The details of the CNN construction and prediction are discussed in the following sections.

3.1. Architecture of convolution neural network

The overall architecture of CNN used in this paper is presented in Fig. 6, which contains the input layer, convolution layer, activation layer, pooling layer, dropout layer, full connected layer, and regression layer. The convolution, activation, and pooling layers are always assembled as a layer set. The input data is first calculated by the convolution layer to extract a series of feature maps, which are then processed by activation function to make the CNN fit the nonlinear problem. Usually, the outputs of the preceding layer are still large and contain too much reductant information, so the pooling layer is adopted to reduce the sizes of the feature maps. To avoid overfitting, a dropout layer is set to remove partial neurons randomly. At last, the full connected layer is applied to make the results suitable for regression analysis. According to Gupta et al. [75] and He et al. [76], the design of CNN configuration plays an essential role in the prediction performance and the computational cost. Hence, this paper will conduct the CNN configuration discussion in Section 4.1. Other details of CNN architecture are discussed as follows.

The convolution layer is the most distinguished characteristics of CNN. Fig. 7 demonstrates the convolution operation on a 2D input I



(b) Comparison between Simulate Spectrum and Davenport Spectrum

Fig. 3. Wind Speed Simulation and Spectrum Comparison.

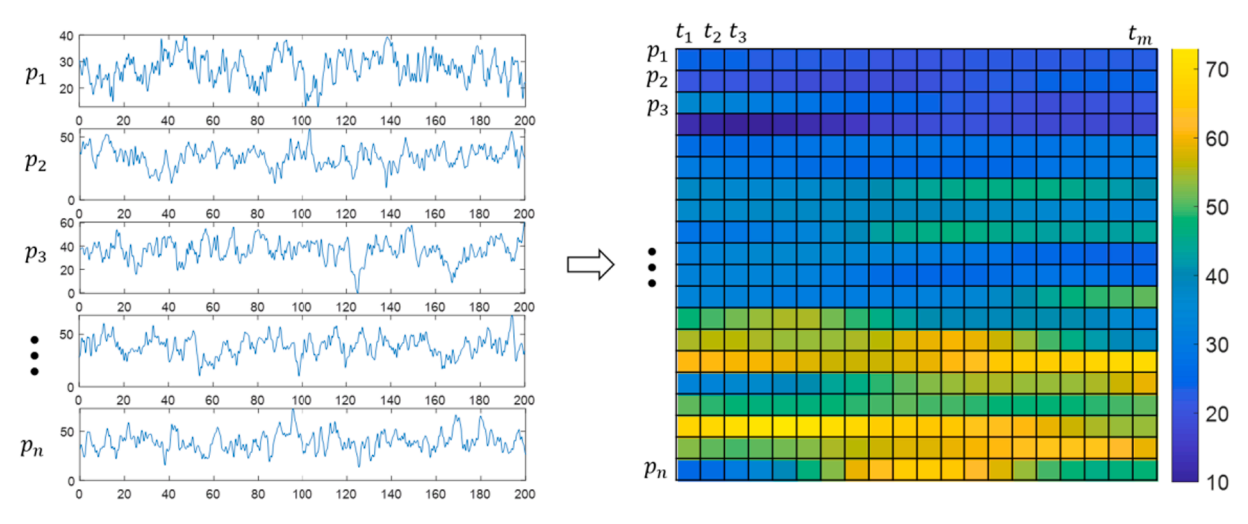


Fig. 5. 2-Dimension Feature of Wind Speed.

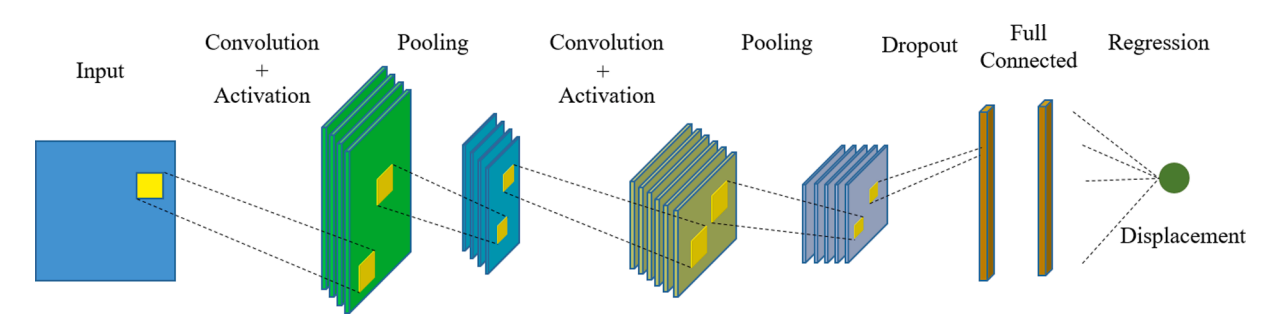


Fig. 6. Architecture of CNN.

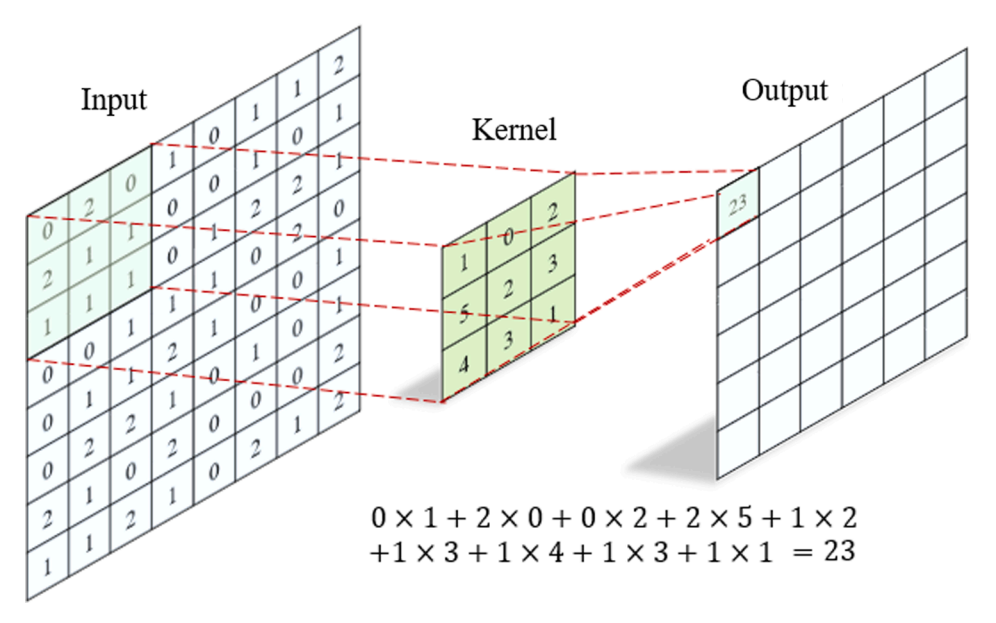


Fig. 7. Illustration of Convolution Operation.

using a 2D kernel K with the size of $m \times m$. If assuming that the weight of kernel K is w(s,t), and the local values of I is f(x-s,y-t), the output of the local convolution operation is then derived as Eq. (12). Subsequently, moving the kernel with a constant step, called as stride, a new image is derived and known as a feature map. To make the feature map representative, N kernels are set to process at the same time. Consequently, N feature maps are obtained. The configuration of kernel size

and number of kernels will be discussed in Section 4.1.

$$g(x,y) = \sum_{s=-a}^{a} \sum_{t=-b}^{b} w(s,t) f(x-s,y-t)$$
 (12)

However, no matter what the kernel size is and how many kernels there are, the convolution operation is a weight sum model and cannot process the nonlinear problem. To address this issue, a leaky rectified

linear unit (Leaky ReLU) is introduced in this research as the activation function. Compared to other activation functions (i.e., Sigmoid, Tanh), Leaky ReLU has couples of superiorities, such as no saturation, computational efficiency, and fast convergence. Meanwhile, since it assigns a non-zero value to the negative input, the gradient update never fails in the weights learning stage. Eq. (13) is the expression of Leaky ReLU, which maps the linear input z to a nonlinear output s(z).

$$s(z) = \max(0.01x, x) \tag{13}$$

To reduce the reductant parameters and avoid overfitting, the pooling layer is designed after the activation layer. There are two primary pooling layers: average pooling and max pooling. Although both of them are down sampling operations, the latter has better performance of feature extraction as it keeps most distinguishable values. Thus, the max pooling is selected in this paper. The principle of the max pooling operation is illustrated in Fig. 8, which can also be understood as subsampling feature maps. Similar to the convolution operation, a predefined window is used to scan the input matrix, and the maximum value located in the window is extracted as the output. The pooling operation can efficiently reduce the sizes of feature maps.

Unlike the classification problem, this paper adopts the CNN to predict the tower top displacement value. Therefore, the output layer of CNN is designed as a regression layer, which uses half-mean-squared-error as the loss function, which is shown in Eq. (14).

$$loss = \frac{1}{2} \sum_{i=1}^{R} (y_{ii} - y_i)^2$$
 (14)

where y_{ii} is the target output, y_i is the prediction, and R is the number of prediction.

3.2. CNN surrogate model development to predict infrastructural wind response

To simulate the dynamic response of the transmission tower, this paper develops an improved CNN that can predict the top displacement of the transmission tower. As mentioned in the previous section, the inducement of the transmission tower's displacement is the wind speed. Hence, CNN utilizes the wind speed as the input and the displacements at the top of the tower as the output. In this paper, the wind speed is denoted as $V = \{v_{t_1}, v_{t_2}, \cdots, v_{t_i}, \cdots\}$, in which $v_{t_i} = \{v_{p_1}, v_{p_2}, \cdots, v_{p_j}, \cdots\}_{t_i}^T$ represents the wind speed happened at different point p_j in the tower at the time t_i . The displacement at the top point of the tower is denoted as $U = \{u_{t_1}, u_{t_2}, \cdots, u_{t_i}, \cdots\}$, in which u_{t_i} is the displacement at time t_i . CNN is developed to map the wind speed V to the top displacement U.

Since the damping exists in the simulation of dynamic response, the u_{t_i} is the result of a period of wind load. Thus, this paper uses a period of wind speed to predict the displacement. Fig. 9 illustrates the mapping

relation between the V and U. A window with the width of w is defined and moved along the time axis step by step. The wind speed $x_i^w = \{v_{i+1}, v_{i+2}, \cdots, v_{i+w}\}$ located in the window is regarded as a stack. Next stack is expressed as $x_{i+1}^w = \{v_{i+2}, v_{i+3}, \cdots, v_{i+w+1}\}$.

Since the tower used in this paper is divided into 5 parts, the dimension of wind speed V in spatial direction is only 5, which is relatively small for the input of CNN. Hence, each window stack x_i^w is resized by cubic interpolation into x with size of $[32 \times 32]$. Then the resized stack x_i of wind speed is used as the input data of CNN. Since the window width w can affect information density of x_i , it will be discussed in Section 4.2.

The displacement at the end of each window stack is denoted as the output data and expressed as $y_i = u_{i+w}$ (Fig. 9). In this scenario, all points in the displacement sequence are sampled, and CNN is become a full sequence simulation CNN. The root mean square error (RMSE) is introduced as the criterion of the prediction performance and shown in Eq. (15), whose nomenclature is the same as Eq. (15).

$$RMSE = \sqrt{\frac{1}{R} \sum_{i=1}^{R} (y_{ii} - y_i)^2}$$
 (15)

4. Parametric study of proposed methodology

The prediction accuracy of CNN is closely related to the CNN configuration, window size selection, and training data scale [77-79]. The depth of the convolutional layers, the kernel size, and numbers are three essential indexes of the CNN configuration. Considering the information density's impact on the data structure and the damping ratio's impact on the physical structure, the window size is another critical choice which may jeopardize the accuracy. The training data set scale is also explored to balance the computational time and calculation accuracy.

4.1. Impact of CNN configuration on the prediction performance

CNN configuration involves several sets of parameters, which can affect the performance in the prediction of structural dynamic response. Notably, the network depth (number of layers), width (number of kernels), and kernel size are the three most important variables that can dramatically change the prediction accuracy and computational time [80-82]. He and Sun [76] demonstrated that the tradeoff among the network depth, width, and kernel size is imperative to achieve competitive accuracy with constrained time. However, limited studies about the CNN application in structural dynamic response discuss the configuration influence on the prediction performance, let along to analyze the impact of network depth, width, and kernel size.

To select a proper CNN configuration, this paper implements the comparison experiments with different network depths, widths, and

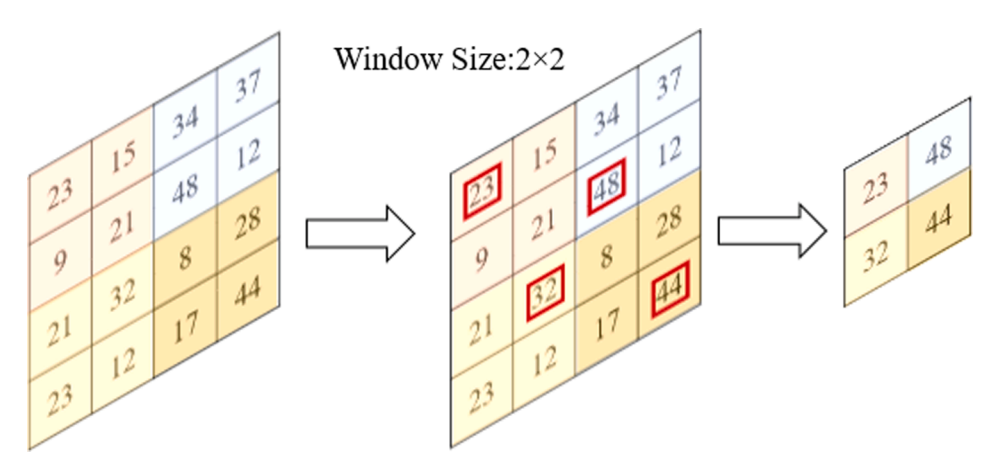


Fig. 8. Illustration of Pooling Operation.

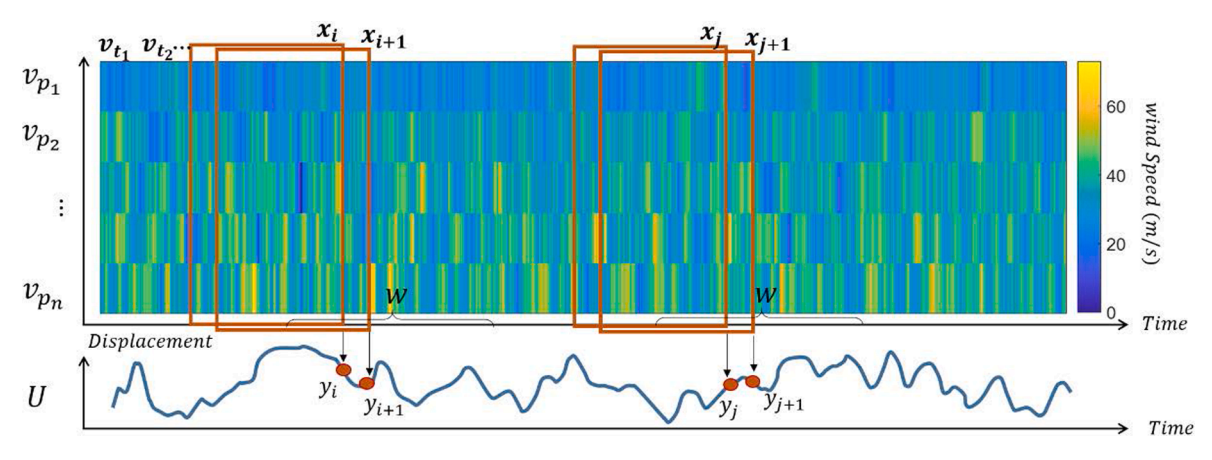


Fig. 9. Mapping Relationship between Wind Speed and Top Displacement.

kernel sizes to figure out the combination of these three parameters with the best prediction performance. As shown in Table 1, four different network depth (3, 4, 5, 6) are designed, and each depth scenario is then classified into six cases. The two values in each cell are the kernel size and width, respectively. If the value in one cell is (7, 16), it means that each kernel size is 7×7 , and there are 16 kernels. The case classification is based on the increase or decrease of width and kernel size along with the network depth.

To generate the dataset of this experiment, 250 samples of the transmission tower's dynamic response during 60 m/s dynamic wind are simulated, in which 170 samples are used as a training dataset, 30 samples are used as a validation dataset, and 50 samples are used as testing dataset. The time length of each sample is 600 s, and the sampling frequency of wind is 10 Hz. The window size selected in this experiment is 10. All calculations involved in this paper are conducted by MATLAB in the computer with the specifications of Intel i7-8920H CPU, Navidia GTX 9470, and 16 GB RAM.

The performances of different CNN configurations are illustrated in Figs. 10 and 11. Fig. 10 (a) is a comparison among the prediction results of Conv3-5, Conv5-1, Conv 6-2, and the ground truth in 600 s. Fig. 10 (b) zooms the comparison from 100 s to 200 s and 110 s to 130 s. The prediction results of Conv3-5 and Conv5-1 show not only the same trend but also a small discrepancy. Conv6-2 captures the primary pattern of the top displacement with the ground truth, but the difference is more significant. In Fig. 11, it demonstrates that all training, validation, and testing RMSE are influenced by the network depths, widths, and kernel sizes simultaneously. However, in each depth, there are some cases with low RMSE. The lowest training RMSE (0.0153) happens in Conv3-5 and Conv5-1. The highest RMSE (0.026) appears at Conv6-2. When considering the training time and testing time, they both increase with the network depth (Fig. 11 (d) and (e)). The training and testing time of Conv6-2 is about twice that of Conv3-5. This phenomenon is caused by the dramatic increase of parameters involved in CNN if the network goes deeper. The computational advance of Conv3-5 is more remarkable when analyzing a large amount of dynamic response of the transmission tower.

4.2. Impact of window size on the prediction performance

As noted above, before training the network, the raw time history data of wind speed and corresponding displacement is preprocessed by a predefined window and resized to uniform data size. It is intrinsic that different window sizes can produce different information densities of the training data, which may consequently affect the prediction performance of CNN. Hence, a comparison study is conducted to discuss the impact of window size on the prediction. Considering the physical properties of the preprocessed dataset, the window size is discussed under two dependencies: (1) sampling frequency, which controls the

data density during the simulation of dynamic wind speed, and (2) damping ratio, which controls the temporal dependency between the wind input and transmission tower response out.

In the sensitivity analysis, a low mean wind speed of 25~m/s and a high wind speed of 60~m/s at the height of 10~m are respectively used to simulate the dataset. The dataset is arranged similarly to the preceding section (65% for training, 15% for validation, 20% for testing). The time length of each sample is also 600~s. Conv3-5, the best CNN configuration from the previous section, is chosen. Then, different window sizes are applied to cut the dataset before training the CNN.

4.2.1. Impact of sampling frequency to window size selection

Since the information density in the time history data is determined by the sampling frequency of wind speed, two kinds of frequency, 10 Hz and 50 Hz, are applied in wind simulation. 7 different window sizes are chosen: 5, 10, 20, 40, 60, 80, 100. Fig. 12 illustrated the experimental results (training, validation, and testing RMSE) under different window sizes during different wind speed and sampling frequency. The x-axis denotes the data points included in each window. Each line in Fig. 12 represents a wind speed (25 m/s or 60 m/s) with a sampling frequency (10 Hz or 50 Hz). Fig. 12 demonstrates the following findings:

- (1) For different window size comparison, the smallest RMSE always happens around the window size of 10 data points. In some cases (wind speed 60 m/s-sampling frequency 50 Hz), the smallest RMSE is not at exactly 10 data points per window, but the RMSE value at 10 data points per window is within a small difference (0.001) to the smallest RMSE.
- (2) For different wind speed comparisons, the RMSEs in the cases with a wind speed of 25 m/s are consistently less than the cases with a wind speed of 60 m/s. Since the RMSE is a standard deviation between predictions and the true values, the smaller value has smaller RMSE if using the same prediction system. Thus, the wind speed 25 m/s cases, which induces small displacement of the transmission tower, presents better performance compared with the wind speed 60 m/s cases.
- (3) For different sampling frequency comparison, the cases of 50 Hz have smaller RMSEs than the cases of 10 Hz. As stated above, the time length of raw data is 600 s, so 50 Hz cases contain 30,000 data points, while 10 Hz cases contain 6000 data points. Thus, compared to 10 Hz cases, 50 Hz cases produce more dataset for training, which means a better prediction performance.

4.2.2. Impact of damping ratio to window size selection

Damping ratio, which influences the oscillation of a system, can be another aspect to consider its impact on the window selection. For the vibration of a transmission tower, different damping ratio impacts its period of decay. Since wind load is time-dependent, it is crucial to

Table 1
CNN configuration with different network depth, width and kernel size.

Case #	Conv1 (kernel size, kernel number)	Conv2 (kernel size, kernel number)	Conv3 (kernel size, kernel number)	Conv4 (kernel size, kernel number)	Conv5 (kernel size, kernel number)	Conv6 (kernel size, kernel number)
Depth: 3 Conv3-	3, 8	5, 16	7, 32	_	_	_
1 Conv3-	3, 32	5, 16	7, 8	_	_	_
2 Conv3-	5, 8	5, 16	5, 32	_	_	-
3 Conv3- 4	5, 32	5, 16	5, 8	-	-	-
Conv3-	7, 8	5, 16	3, 32	-	-	-
Conv3-	7, 32	5, 16	3, 8	-	-	-
Depth: 4 Conv4-	3, 8	5, 16	7, 32	11, 48	_	-
Conv4-	3, 48	5, 32	7, 16	11, 8	-	-
Conv4-	5, 8	5, 16	5, 32	5, 48	-	-
Conv4-	5, 48	5, 32	5, 16	5, 8	-	-
Conv4- 5	11, 8	7, 16	5, 32	3, 48	-	-
Conv4- 6	11, 48	7, 32	5, 16	3, 8	-	-
Depth: 5 Conv5- 1	3, 8	5, 16	7, 32	11, 48	11, 48	-
Conv5- 2	3, 48	5, 48	7, 32	11, 16	11, 8	-
Conv5-	7, 8	7, 16	7, 32	7, 48	7, 48	-
Conv5-	7, 48	7, 48	7, 32	7, 16	7, 8	-
Conv5- 5	11, 8	11, 16	7, 32	5, 48	3, 48	-
Conv5- 6 Depth: 6	11, 48	11, 48	7, 32	5, 16	3, 8	-
Conv6-	3, 8	5, 16	7, 32	11, 48	11, 48	11, 48
Conv6-	3, 48	5, 48	7, 48	11, 32	11, 16	11, 8
Conv6-	7, 8	7, 16	7, 32	7, 48	7, 48	7, 48
Conv6- 4	7, 48	7, 48	7, 48	7, 32	7, 16	7, 8
Conv6- 5	11, 8	11, 16	11, 32	7, 48	5, 48	3, 48
Conv6- 6	11, 48	11, 48	11, 48	7, 32	5, 16	3, 8

consider the wind load's impact on the time length, in other words, the impact of window selection. According to the discussion of sampling frequency in 4.2.1, window selection is consistent for both 50 Hz and 10 Hz. In this experiment, only 10 Hz sampling frequency of 25 m/s and 60 m/s wind speeds are tested. Four different damping ratios of transmission tower are selected: 0.01, 0.02, 0.05, 0.1.

Fig. 13 presents the RMSEs of training, validation, and testing dataset of two wind speeds with different damping ratios. It is evident that the smallest RMSEs always happen around the data point of 10, which is the same as the discussions in the previous section. Similarly, the RMSEs in the cases of 25 m/s are better than the cases of 60 m/s, which has been analyzed in the previous section. In summary, the data point of 10 is an optimal choice for the window size, which will be further employed in the following sections.

4.3. Impact of training sample size on prediction performance

The selection of training sample size is also a tradeoff between the prediction performance and computational time, especially when expanding the mean wind speed from one certain value to a broad range. Thus, this paper experiments with the wind speeds of 25 m/s and 60 m/s, both of which have 10 Hz sampling frequency. For each wind speed, this paper uses different sample sizes to train the network, 70% of which are used as a training dataset, and 30% are validation dataset. To conduct the comparison, the testing dataset is consistent with 50 samples.

Fig. 14 summarizes the RMSEs under different sample numbers with 25 m/s and 60 m/s. With the increase of the sample number, the RMSE for both 25 m/s and 60 m/s decreases with a similar trend. Although more data can generate a network with high accuracy, it demonstrates that when the sample number reaches 100, the RMSE fluctuates in a 10^{-3} range. At the same time, the computational training time can save half compared with 200 samples. Therefore, 100 samples are the proper training size for one wind speed.

In summary, the CNN configuration, window size, and training data scale all impact the prediction performance, including the prediction error and computational time. Based on a set of comparative studies in this section, Conv3-5 is chosen as the proper CNN configuration; 10 data length is selected as the window size; and 100 samples of training set is considered as a good trade-off between computational time (both in running numerical simulation to prepare the training data and network training) and accuracy.

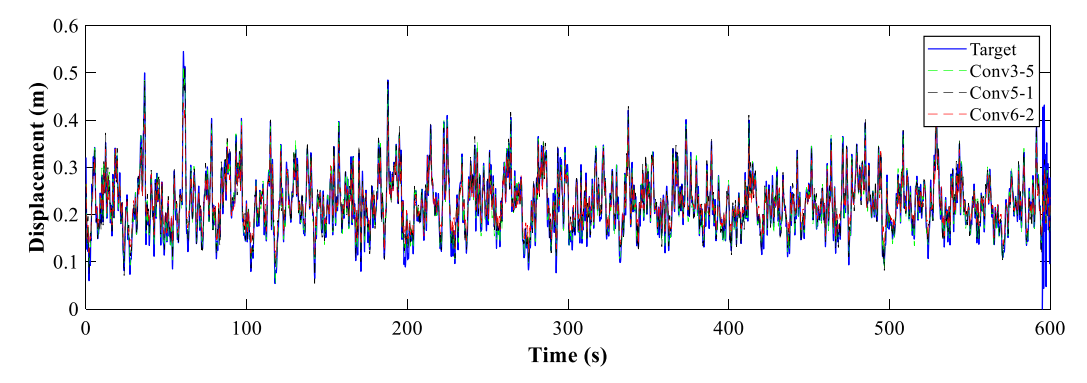
5. Results and discussion

Based on the previous experiments and analysis, the trained CNN is employed to predict the top displacement during certain dynamic wind load. As transmission towers spread broadly in a region, it is vital to develop a trained CNN, which can predict a transmission tower's performance of different wind speeds. The wind speeds from 15 m/s to 70 m/s with 5 m/s increase are selected to generate 200 samples at each wind speed, half of which are used as training, and the rests are for testing. Conv3-5 is chosen as the desired CNN, and Conv6-2 is chosen as a comparison to illustrate the importance of CNN configuration. Window size of 10 and 100 data points are also employed to test the efficiency of the window size. There are four kinds of CNN in this analysis: 1) Conv3-5 with 10 data points window size; 2) Conv3-5 with 100 data points window size; 4) Conv6-2 with 100 data points window size.

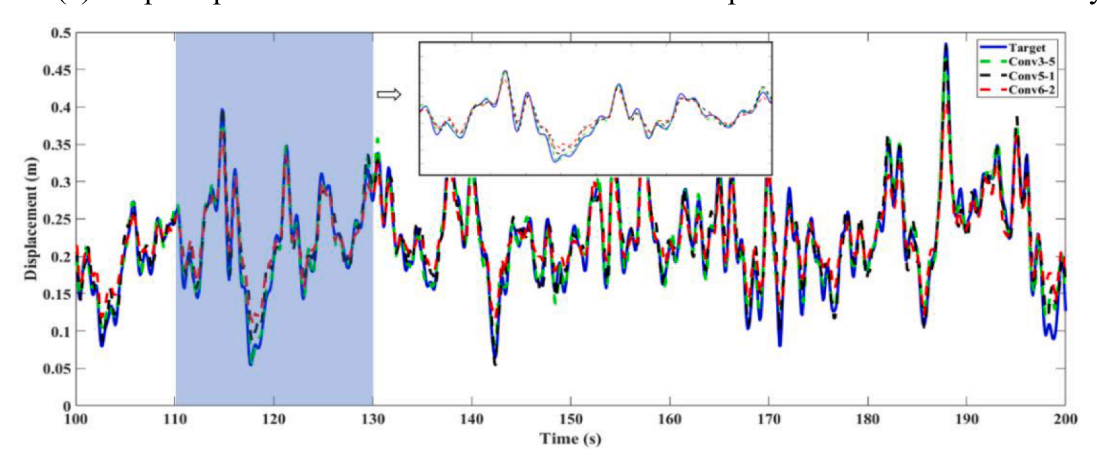
The error analysis and result discussion include three parts: 1) Evaluate the accuracy of the CNN surrogate model through analyzing the deviation of prediction and ground truth; 2) Evaluate the effectiveness of the CNN surrogate model using the predicted peak displacement to develop a fragility model; 3) Assess the robustness of the CNN surrogate model using two random inputs generated by a random wind profile and a Kaimal spectrum; 4) CNN configuration with better performance will be tested on the wind load from different directions.

5.1. Surrogate model accuracy evaluation on time history prediction error

To validate the window size and the configuration optimized in the sensitivity analysis, and to evaluate the accuracy of the proposed design, CNN models constructed with Conv3-5, Conv6-2, and two different window sizes are trained and compared. Table 2 compares the error and computational time of each CNN. As can be seen, with the optimal CNN configuration, Conv3-5, and window size of 10, the RMSE and computational time are the best among four cases. Comparing to Conv6-2, Conv3-5 can save half of the computational time with twice accuracy improvement. To further analyze the error distribution of each network, the error histogram of all datasets, and the regression of the testing dataset are plotted and presented in Fig. 15. Conv3-5 with window size

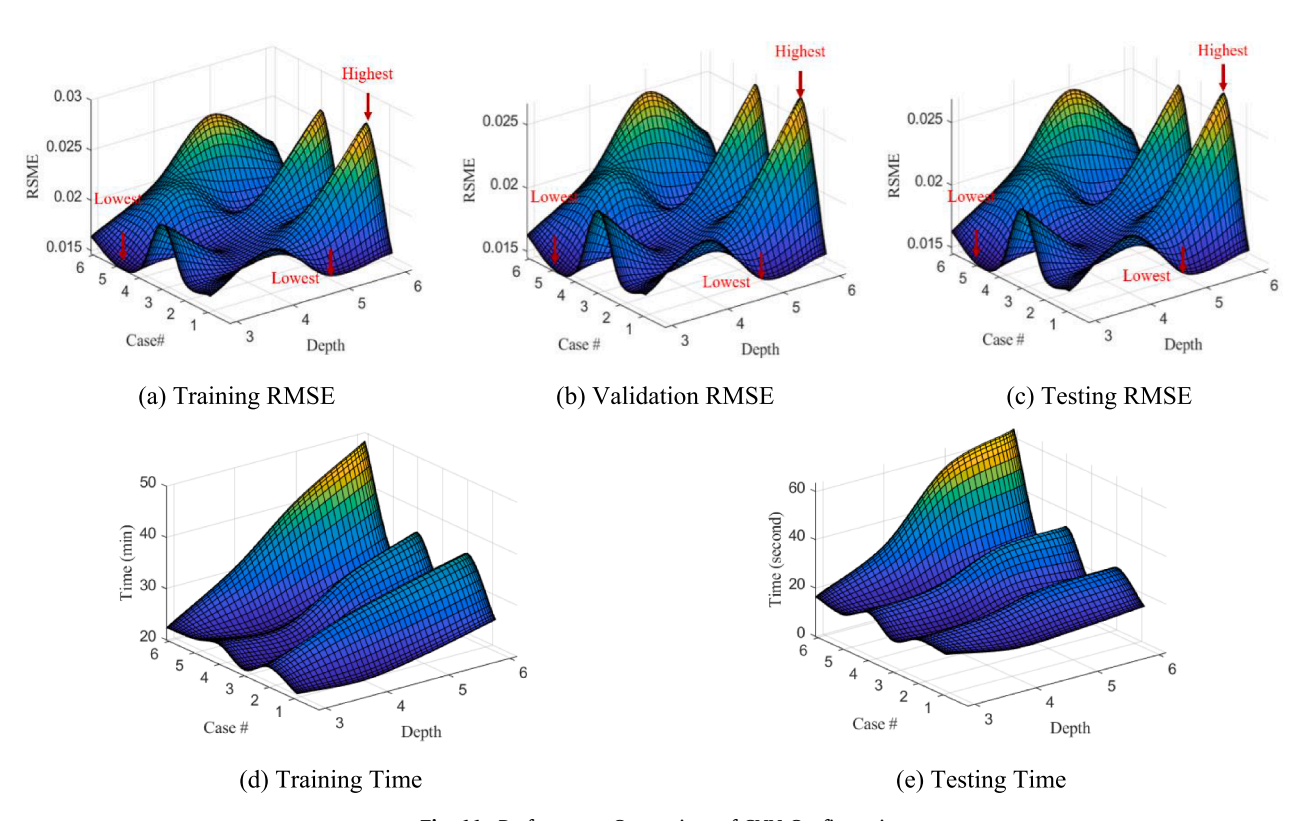


(a) Top Displacement Prediction Performance Comparison in 600s Time History



(b) Zoomed-in Prediction Comparison between 100s-200s

Fig. 10. Top Displacement Prediction Performance Comparison.



 $\textbf{Fig. 11.} \ \ \textbf{Performance Comparison of CNN Configuration.}$

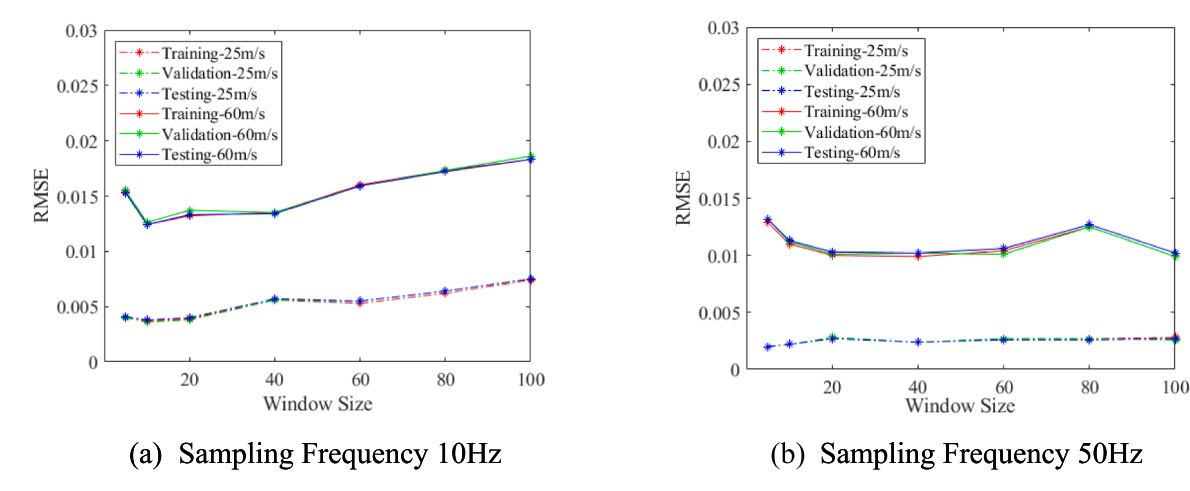


Fig. 12. Window Size Comparison for Sampling Frequency.

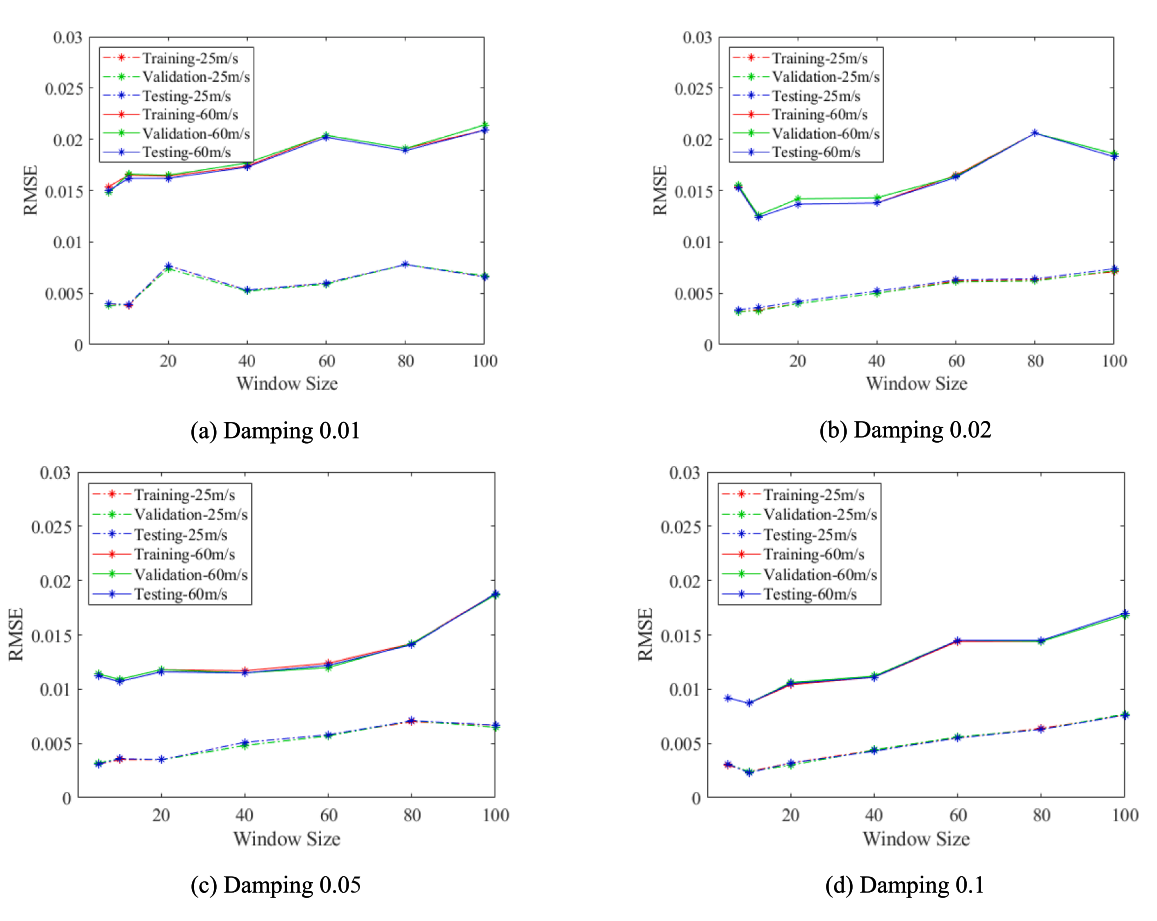


Fig. 13. Window Size Comparison for Damping.

of 10 has the optimal distribution because of the smallest deviations of predictions and ground truth. Also, its fitted line for the predicted values in the testing dataset is the closest to the true line among the four cases. Therefore, considering the results from both Table 2 and Fig. 15, it can be concluded that the configuration of CNN plays a vital role in predicting the top displacements of transmission tower under different wind speeds, and Conv3-5 with a window size of 10 data points has the best performance. However, from the qualitative analysis of RMSE to different CNN training parameters, the results indicate the maximum error is 0.0264 and minimum of 0.0103. As RMSE does not give a good indicator on the acceptance of the accuracy level, further discussions are followed to evaluate CNN surrogate model performance.

5.2. Surrogate model effectiveness evaluation on the fragility model development

The maximum top displacement of a transmission tower is also a cared index to estimate the tower's failure. When the top drift exceeds the limit of a transmission tower, the tower is considered to collapse. Fig. 16(a) illustrates the maximum top displacement prediction error for each case. The median prediction error for both Conv3-5 with 10 data length and Conv3-5 with 100 data length is close to 0. Half of the prediction error is smaller than 0.025 m. For both cases using Conv6-2, the median prediction error is clearly higher than the previous two cases, and the error also spread in a larger range.

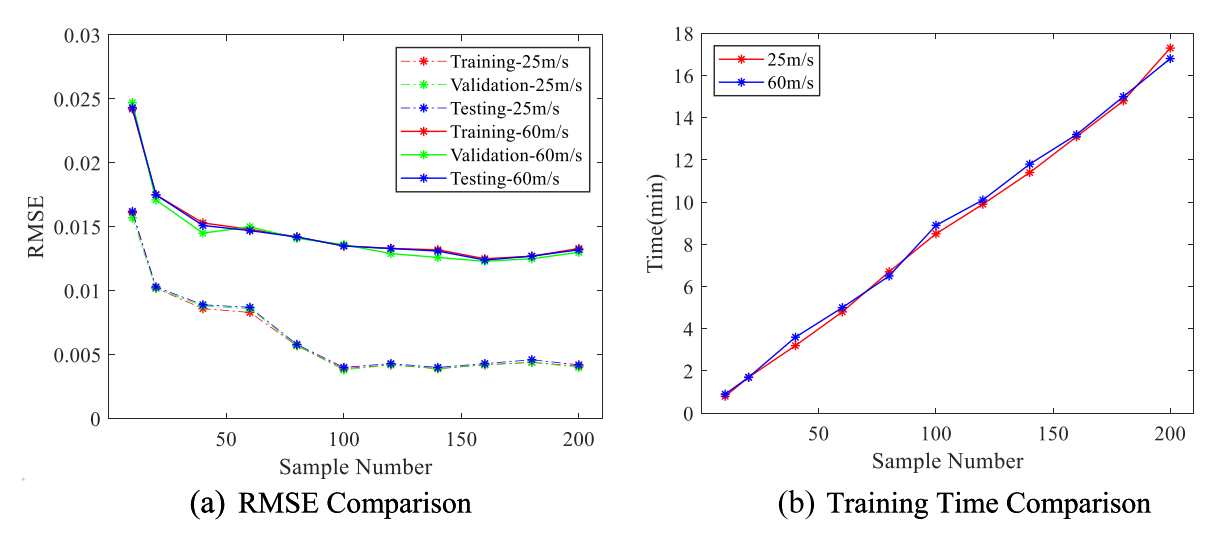


Fig. 14. RMSE and Training Time Comparison.

Table 2
Error and Computational Time Comparison.

	Window Size	RMSE_Train	RMSE_Validation	RMSE_Test	Training Time	Testing Time
Conv3-5	10	0.0101	0.0099	0.0103	129.5	23.1
Conv3-5	100	0.0130	0.012	0.0130	127.6	25.4
Conv6-2	10	0.0218	0.0217	0.0219	239.8	31.3
Conv6-2	100	0.0262	0.0270	0.0264	240.0	30.1

Another essential index to evaluate the efficiency of CNN is the fragility curve, which expresses the likelihood of a structure's damage under different wind speeds as Eq. (16).

$$F_R(V) = P[D > LS|V_{10} = V]$$
 (16)

where $F_R(V)$ is the failure probability of a transmission tower under a certain wind speed V; LS is the limit state of a transmission tower. D is the tower's response. In this paper D is the top displacement of the transmission tower. For the wind-induced failure analysis of the transmission tower, the top displacement is usually chosen as an index to evaluate its collapse [74]. V_{10} is the mean wind speed ranging from 15 m/s to 70 m/s.

In this section analysis, the performance of the CNN model is evaluated by comparing the developed fragility curve to the baseline fragility curve. The true fragility curve developed following conventional Monte Carlo simulation is recorded and shown in Fig. 16(b) with wind speeds from 15 m/s to 70 m/s. The four CNN also generate corresponding fragility curves using predicted transmission tower response. It demonstrates that the fragility curve generated by Conv3-5 is close to the true fragility curve. The only discrepancy happens when the wind speed is 45 m/s. For Conv6-2's two cases, the prediction results are considerably different as compared to both results in Conv3-5 or the ground truth. Therefore, it indicates that 0.02–0.025in the RMSE cannot yield an acceptable performance.

5.3. Surrogate model robustness evaluation with random wind profile and wind spectrum

Thirdly, in order to validate the robustness of the developed surrogate model to the uncertainties in wind profiles and wind spectrums, two samples generated by a random wind profile and a Kaimal spectrum are chosen to test the robustness of the trained network. The random mean wind speed for the testing input is 32.6 m/s at 10 m as shown in Fig. 17. The rest profiles are from the trained profiles. Fig. 18 compares the prediction performance of the four cases. It demonstrates that Conv3-5

with window size 10 data points has the best fitness of the ground truth. Conv6-2 can capture the basic trend of the dynamic response while it shows some discrepancy with an accurate value. It proves that this Conv3-5 network with window size 10 data points can effectively predict the time history response of a transmission tower for random wind speeds. It demonstrates that the profile uncertainty can be well considered by the proposed surrogate model.

To investigate the robustness of the proposed surrogate model in tolerating the uncertainty caused by various spectrums, one wind loading input generated by Kaimal spectrum (Eq. (17)) [83] is tested by this surrogate model, the Kaimal spectrum is expressed as:

$$S_{\nu}(z,f) = \frac{200f_* V_*^2}{f(1+50f_*^{5/3})^f_*} = \frac{fz}{\overline{V}}, V_* = \kappa \overline{V}_{10}^2$$
(17)

where V_* is the friction velocity; f_* is Monin coordinate.

The comparison between Kailmal and Davenport spectrums are presented in Fig. 19, the frequency domain difference is clearly demonstrated in the first 0.2 Hz which is the domain frequency in the wind loading. Fig. 20 shows the prediction results of four CNN configuration that is trained only by the wind loading generated with Davenport spectrum. The predicted response using Cov3-5 (w = 10) yields an RMSE of 0.0066 from the true response, compared to RMSE of 0.0099 in the training (Table 2), the performance accuracy is consistent. Therefore, it can be concluded that the developed surrogate model can capture the wind profile and spectrum uncertainty.

Table 3 summarizes the RMSEs for the cases generated by the random wind profile and the Kaimal spectrum under the CNN configurations trained in previous sections. The results obtained in the comparison align with the optimized CNN configuration, that Cov 3–5 with window size of 10 data points outperform the rest of the configurations.

5.4. Surrogate model robustness evaluation with wind loads from different directions

Finally, to validate the robustness of this approach, the surrogate

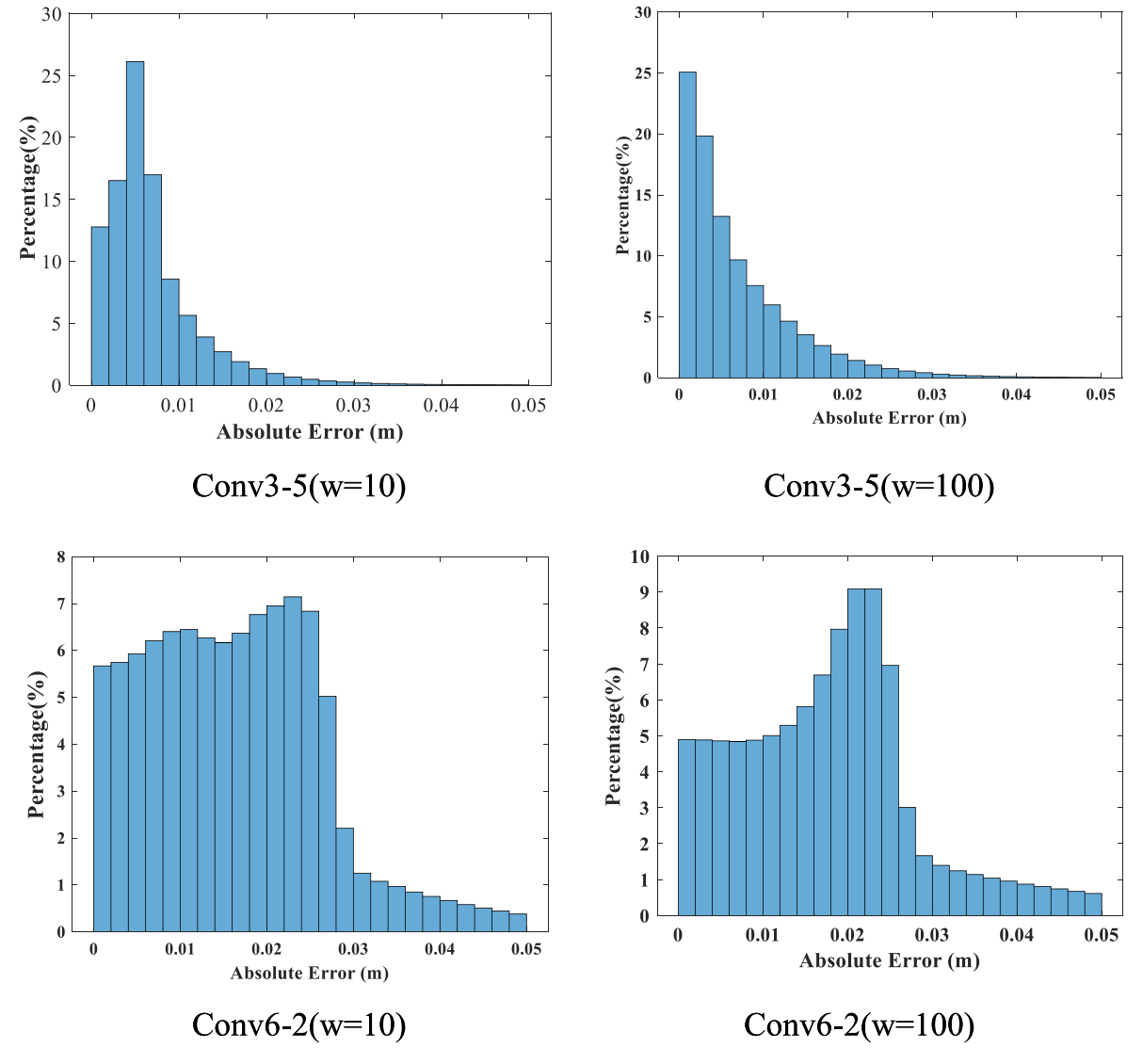


Fig. 15. Error Histogram and Regression Comparison.

model of the transmission tower during the wind loads from different directions are tested. Based on the previous results, Conv3-5 with 10 data point window size has the best performance to develop the surrogate model. Therefore, this CNN configuration will be employed to develop the surrogate model of the transmission tower when the wind loads are from 30 degrees, 45 degrees, 60 degrees, 90 degrees as Fig. 21 (a) demonstrates.

Table 4 summarizes the training, validation and testing RMSE from different wind directions. It clearly demonstrates with proper CNN configuration and window size selection, the surrogate model can predict the transmission tower's performance during the wind load from different wind directions.

6. Conclusion

This paper proposed a novel method to predict the time history response of a standalone transmission tower under complex wind input using convolutional neural network (CNN). By converting the time and spatial information of wind into a surface wave, CNN can predict the dynamic response of transmission tower with satisfying accuracy. This study leads to the following conclusions:

- (1) CNN can capture the time and spatial correlation of the complex wind input and predict the dynamic performance of the transmission tower successfully.
- (2) CNN configuration with different network depth, width, and kernel size impacts the prediction accuracy and computational time at the same time. In the study, Conv3-5 outperforms other configuration in predicting the dynamic response of the transmission tower in a broader wind speed range. Both RMSE and computational efficiency is largely improved compared to Conv6-2.
- (3) Window size also influences the accuracy of time history prediction. According to a set of experiments considering different sampling frequency and damping ratio, 10 data point window size is selected as the most favorable window length. Physical property of the transmission tower, such as damping ratio, does not impact the optimal selection of the window size.
- (4) In order to choose a proper data scale with sufficient accuracy and limited computational time, a group of sample numbers is trained and compared. 100 samples for each wind speed are the ideal data scale to train a promising CNN.
- (5) Compared with window size, CNN configuration influences both the time history prediction and the extreme value and fragility

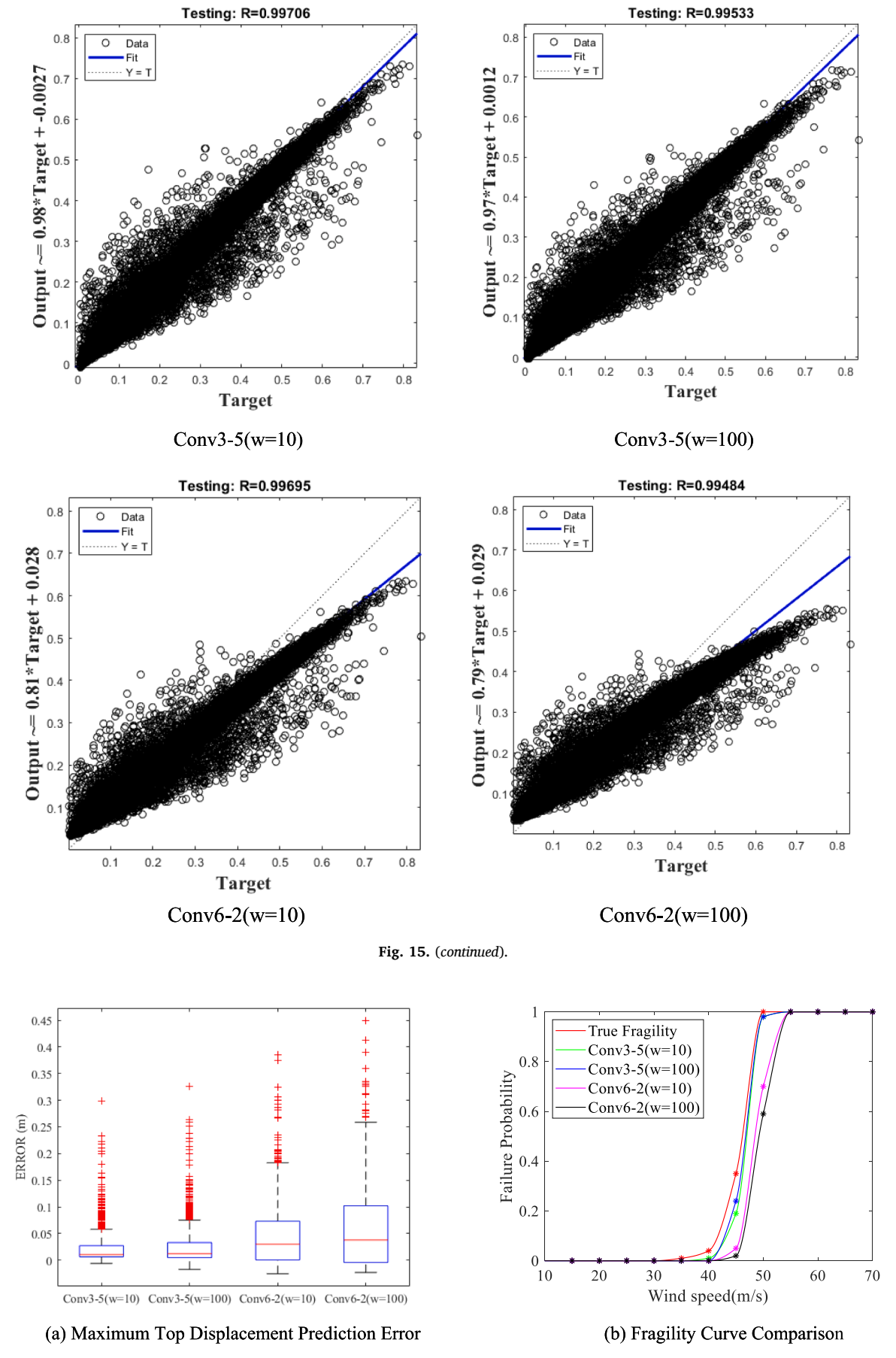


Fig. 16. Extreme Condition Comparison.

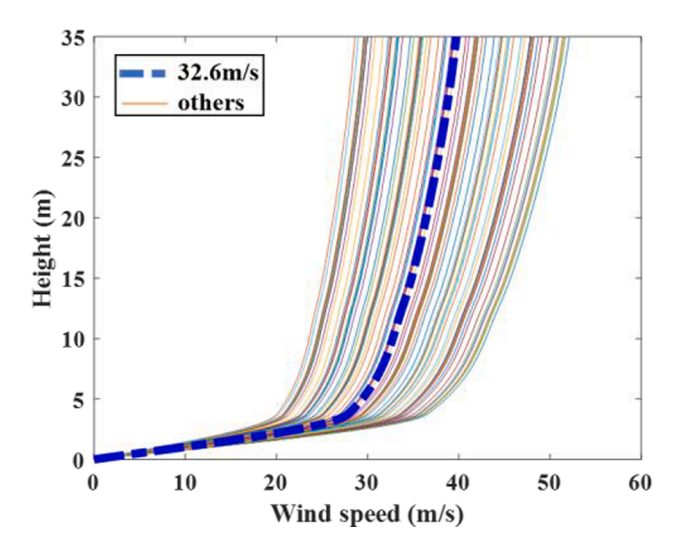


Fig. 17. Wind Profile Distribution of Various Mean Wind Profile.

analysis of the transmission tower. Window size selection impacts the accuracy of the time history while it tolerates the discrepancy when only considering the extreme value and fragility analysis.

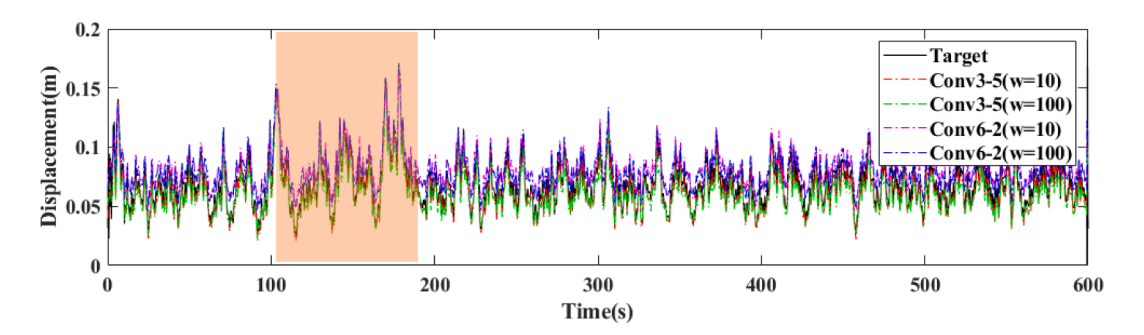
- (6) This surrogate model is robust to the wind loading uncertainties that are caused by the widely distributed wind profiles and various wind spectra. The presented results are promising as the RMSEs between the predicted dynamic responses and the ground truth are compatible with the RMSEs in the training.
- (7) With Cov3-5 and 10 data point window size selection, this approach can successfully predict the dynamic response of the

- transmission tower when the wind loads are from different directions.
- (8) By transferring the time and spatial correlation of the wind loads into an image, the powerful image process network, CNN, can be employed to predict the structure's dynamic response during the wind load. It provides a new insight to deal with the time and spatial correlation of the wind loads and applies this approach to the other structures.

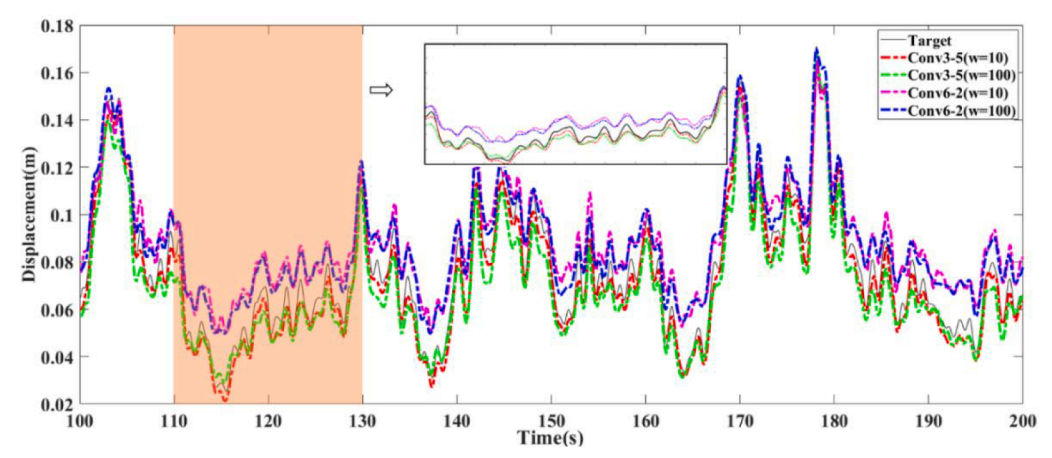
Overall, this paper provides a thorough discussion of the CNN development for the time history response prediction of the transmission tower. With proper CNN configuration and training data, this surrogate model can successfully capture the wind loading uncertainties from the distributed wind profiles and spectra, which is critical for the realistic hurricane meteorological data. One limitation of the method that needs to be noted, is that the accuracy of CNN depends highly on the representativeness of the training data. In this study, 100 samples with 600 s time history are proved to be sufficient for training. Therefore complex material and geometric nonlinearity of transmission tower and towerline interaction is not considered due to computational cost in generating the training data. In the future, advanced sampling methods will be studied to reduce the required training sample, and application with different nonlinearity will be addressed.

CRediT authorship contribution statement

Jiayue Xue: Conceptualization, Methodology, Formal analysis, Validation, Writing - original draft. **Zhongming Xiang:** Conceptualization, Methodology. **Ge Ou:** Supervision, Conceptualization, Writing - review & editing, Funding acquisition.



(a) Top Displacement Prediction Performance Comparison



(b) Zoomed-in Prediction Comparison between 100s-200s

Fig. 18. Top Displacement Prediction Performance Comparison.

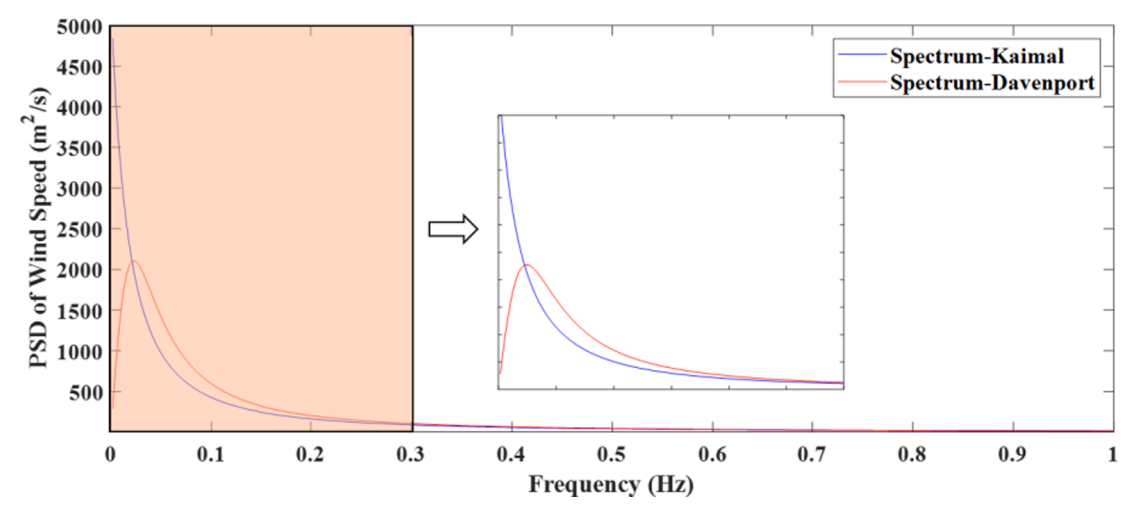


Fig. 19. Comparison between Kaimal spectrum and Davenport spectrum.

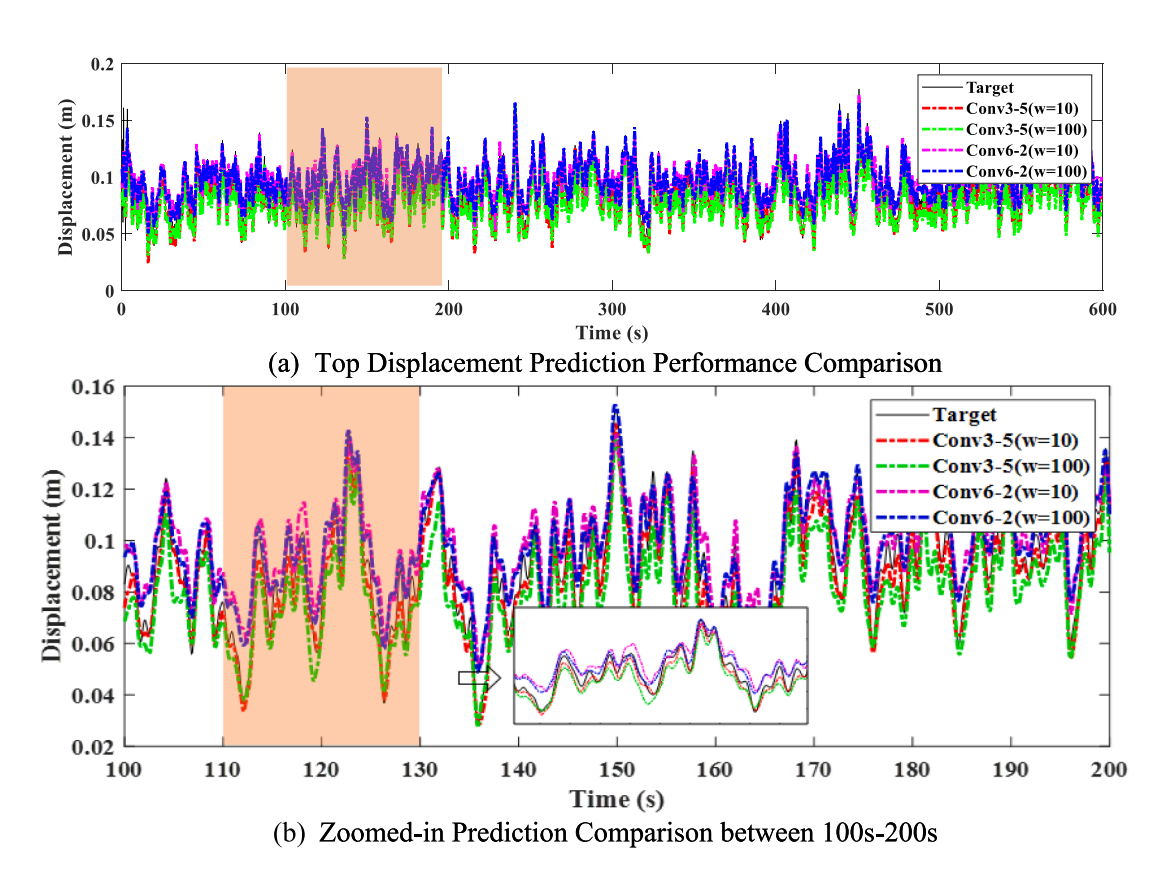
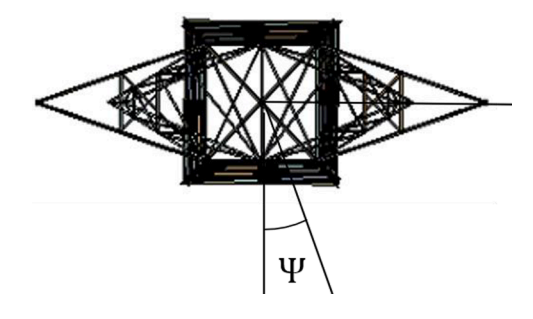


Fig. 20. Top Displacement Prediction Performance for Wind Speed Simulated by Kaimal Spectrum.

Table 3RMSEs for Wind Profile and Spectrum Uncertainty Prediction.

	Window Size	RMSE _Test (Wind Profile uncertainty)	RMSE _Test (Spectrum uncertainty)
Conv3- 5	10	0.0055	0.0066
Conv3- 5	100	0.0084	0.0118
Conv6- 2	10	0.0102	0.0118
Conv6-	100	0.0137	0.0140



 $\textbf{Fig. 21.} \ \ \textbf{Wind load from different directions.}$

Table 4 RMSEs for different wind directions.

	0 Degree	30 Degree	45 Degree	60 Degree	90 Degree
RMSE_Train	0.0073	0.0063	0.0055	0.0094	0.0107
RMSE_Validation	0.0077	0.0062	0.0053	0.0097	0.0111
RMSE Test	0.0075	0.0064	0.0056	0.0095	0.0109

Declaration of Competing Interest

The authors declare that they have no known competing financial interests or personal relationships that could have appeared to influence the work reported in this paper.

Acknowledgement

The research work described in this paper was supported by Utah's Technology Catalyst (USTAR), award number 18065UTAG004; and National Science Foundation under award number 1839833 and 2004658.

References

- NERC. (2018). Hurricane Harvey Event Analysis Report, North American Electric Reliability Corporation.
- [2] NOAA. (2018). Hurricane Michael (AL142018), National Hurricane Center Tropical Cyclone Report.
- [3] Alam MJ, Santhakumar AR. Reliability analysis and full-scale testing of transmission tower. J Struct Eng 1996;122(3):338–44.
- [4] Albermani F, Kitipornchai S, Chan RW. Failure analysis of transmission towers. Eng Fail Anal 2009;16(6):1922–8.
- [5] Rao NP, Knight GS, Mohan SJ, Lakshmanan N. Studies on failure of transmission line towers in testing. Eng Struct 2012;35:55–70.
- [6] Fu X, Wang J, Li HN, Li JX, Yang LD. Full-scale test and its numerical simulation of a transmission tower under extreme wind loads. J Wind Eng Ind Aerodyn 2019; 110:110-22.
- [7] Zhang, Z. F., Yang, J. B., Yang, F. L., & Li, Q. H. (2013). Design and Full-Scale Test for Cup-Type Steel Tubular Tower of UHV Transmission Line in Heavy Icing Area. In Advanced Materials Research (Vol. 732, pp. 1074-1080). Trans Tech Publications Ltd.
- [8] Tian L, Guo L, Ma R, Gai X, Wang W. Full-scale tests and numerical simulations of failure mechanism of power transmission towers. Int J Struct Stab Dyn 2018;18 (09):1850109.
- [9] Lee PS, McClure G. Elastoplastic large deformation analysis of a lattice steel tower structure and comparison with full-scale tests. J Constr Steel Res 2007;63(5): 709–17
- [10] Deng HZ, Si RJ, Hu XY, Duan CY. Wind tunnel study on wind-induced vibration responses of a UHV transmission tower-line system. Adv Struct Eng 2013;16(7): 1175–85.
- [11] Liang S, Zou L, Wang D, Cao H. Investigation on wind tunnel tests of a full aeroelastic model of electrical transmission tower-line system. Eng Struct 2015;85: 63–72.
- [12] Xie Q, Cai Y, Xue S. Wind-induced vibration of UHV transmission tower line system: Wind tunnel test on aero-elastic model. J Wind Eng Ind Aerodyn 2017;171: 219–29.
- [13] Edgar TH, Sordo E. Structural behaviour of lattice transmission towers subjected to wind load. Struct Infrastruct Eng 2017;13(11):1462–75.
- [14] Al-Bermani FG, Kitipornchai S. Nonlinear analysis of transmission towers. Eng Struct 1992;14(3):139–51.
- [15] Mara TG, Hong HP. Effect of wind direction on the response and capacity surface of a transmission tower. Eng Struct 2013;57:493–501.
- [16] Fu X, Li HN. Uncertainty analysis of the strength capacity and failure path for a transmission tower under a wind load. J Wind Eng Ind Aerodyn 2018;173:147–55.
- [17] Savory E, Parke GA, Zeinoddini M, Toy N, Disney P. Modelling of tornado and microburst-induced wind loading and failure of a lattice transmission tower. Eng Struct 2001;23(4):365–75.
- [18] Fei Q, Zhou H, Han X, Wang J. Structural health monitoring oriented stability and dynamic analysis of a long-span transmission tower-line system. Eng Fail Anal 2012;20:80-7
- [19] Zhang Z, Li H, Li G, Wang W, Tian L. The numerical analysis of transmission towerline system wind-induced collapsed performance. Mathem Probl Eng. 2013.
- [20] Yang SC, Hong HP. Nonlinear inelastic responses of transmission tower-line system under downburst wind. Eng Struct 2016;123:490–500.
- [21] Panteli M, Mancarella P, Wilkinson S, Dawson R, Pickering C. Assessment of the resilience of transmission networks to extreme wind events. In: 2015 IEEE Eindhoven PowerTech, IEEE, 2015, June, p. 1–6.
- [22] Fu X, Li HN, Li G. Fragility analysis and estimation of collapse status for transmission tower subjected to wind and rain loads. Struct Saf 2016;58:1–10.

- [23] Yang YH, Xin YL, Zhou JJ, Tang WH, Li B. Failure probability estimation of transmission lines during typhoon based on tropical cyclone wind model and component vulnerability model. In: 2017 IEEE PES Asia-Pacific Power and Energy Engineering Conference (APPEEC), IEEE, 2017, November. p. 1–6.
- [24] Kim YS, Kim BT. Prediction of relative crest settlement of concrete-faced rockfill dams analyzed using an artificial neural network model. Comput Geotech 2008;35 (3):313–22.
- [25] Bernier C, Padgett JE. Fragility and risk assessment of aboveground storage tanks subjected to concurrent surge, wave, and wind loads. Reliab Eng Syst Saf 2019;191: 106571.
- [26] Su G, Zhang K, Zhang H, Zhang Y. Deformation prediction of foundation pit using Gaussian process machine learning. In: 2009 Asia-Pacific Conference on Computational Intelligence and Industrial Applications (PACIIA), IEEE, 2009, November, Vol. 1, p. 99–102.
- [27] Kang F, Han S, Salgado R, Li J. System probabilistic stability analysis of soil slopes using Gaussian process regression with Latin hypercube sampling. Comput Geotech 2015;63:13–25.
- [28] Lagaros ND, Tsompanakis Y, Psarropoulos PN, Georgopoulos EC. Computationally efficient seismic fragility analysis of geostructures. Comput Struct 2009;87(19–20): 1195–203.
- [29] Wang Z, Pedroni N, Zentner I, Zio E. Seismic fragility analysis with artificial neural networks: Application to nuclear power plant equipment. Eng Struct 2018;162: 213–25.
- [30] Mangalathu S, Heo G, Jeon JS. Artificial neural network based multi-dimensional fragility development of skewed concrete bridge classes. Eng Struct 2018;162: 166-76
- [31] Vanluchene RD, Sun R. Neural networks in structural engineering. Comput-Aided Civ Infrastruct Eng 1990;5(3):207–15.
- [32] Mukherjee A, Biswas SN. Artificial neural networks in prediction of mechanical behavior of concrete at high temperature. Nucl Eng Des 1997;178(1):1–11.
- [33] Mohammadhassani M, Nezamabadi-Pour H, Suhatril M, Shariati M. Identification of a suitable ANN architecture in predicting strain in tie section of concrete deep beams. Struct Eng Mech 2013;46(6):853–68.
- [34] Ceylan H, Tutumluer E, Thompson MR, Gomez-Ramirez F. September). Neural network-based structural models for rapid analysis of flexible pavements with unbound aggregate layers. In: Proceedings, Sixth International Symposium on Pavements Unbound; 2014. p. 139–47.
- [35] Oh BK, Glisic B, Kim Y, Park HS. Convolutional neural network-based windinduced response estimation model for tall buildings. Comput-Aided Civ Infrastruct Eng 2019;34(10):843–58.
- [36] Su G, Peng L, Hu L. A Gaussian process-based dynamic surrogate model for complex engineering structural reliability analysis. Struct Saf 2017;68:97–109.
- [37] Zhao HB. Slope reliability analysis using a support vector machine. Comput Geotech 2008;35(3):459–67.
- [38] Sainct R, Feau C, Martinez JM, Garnier J. Efficient Seismic fragility curve estimation by Active Learning on Support Vector Machines. 2018. arXiv preprint arXiv:1810.01240.
- [39] Afshari SS, Liang X. Probability Density Evolution Method Enhanced with Machine Learning Techniques for Structural Reliability Analysis. 2019.
- [40] Perera R, Sandercock S, Carnicero A. Civil structure condition assessment by a twostage FE model update based on neural network enhanced power mode shapes and an adaptive roaming damage method. Eng Struct 2020;207:110234.
- [41] Ying W, Chong W, Hui L, Renda Z. Artificial Neural Network Prediction for Seismic Response of Bridge Structure. In: 2009 International Conference on Artificial Intelligence and Computational Intelligence, IEEE, 2009, November, Vol. 2, p. 503-6.
- [42] Lagaros ND, Papadrakakis M. Neural network based prediction schemes of the nonlinear seismic response of 3D buildings. Adv Eng Softw 2012;44(1):92–115.
- [43] Zhang R, Chen Z, Chen S, Zheng J, Büyüköztürk O, Sun H. Deep long short-term memory networks for nonlinear structural seismic response prediction. Comput Struct 2019;220:55–68.
- [44] Bani-Hani KA. Vibration control of wind-induced response of tall buildings with an active tuned mass damper using neural networks. Struct Control Health Monitor: Offic J Int Assoc Struct Control Monitor Eur Assoc Control Struct 2007;14(1): 83–108.
- [45] Dongmei H, Shiqing H, Xuhui H, Xue Z. Prediction of wind loads on high-rise building using a BP neural network combined with POD. J Wind Eng Ind Aerodyn 2017:170:1–17.
- [46] Peterson EW, Hennessey Jr JP. On the use of power laws for estimates of wind power potential. J Appl Meteorol 1978;17(3):390–4.
- [47] Li QS, Zhi L, Hu F. Boundary layer wind structure from observations on a 325 m tower. J Wind Eng Ind Aerodyn 2010;98(12):818–32.
- [48] Bec J. Influence of wind spectrum formula choice on footbridge response. In: 5th international symposium on computational wind engineering; 2010. p. 23–7.
- [49] Snaiki R, Wu T. A semi-empirical model for mean wind velocity profile of landfalling hurricane boundary layers. J Wind Eng Ind Aerodyn 2018;180:249–61.
- [50] Vickery PJ, Wadhera D, Powell MD, Chen Y. A hurricane boundary layer and wind field model for use in engineering applications. J Appl Meteorol Climatol 2009;48 (2):381–405.
- [51] Sucevic N, Djurisic Z. Influence of atmospheric stability variation on uncertainties of wind farm production estimation. European wind Energy conference and exhibition. 2012.
- [52] Constantinescu EM, Zavala VM, Rocklin M, Lee S, Anitescu M. A computational framework for uncertainty quantification and stochastic optimization in unit commitment with wind power generation. IEEE Trans Power Syst 2010;26(1): 431-41.

- [53] Shiau BS, Chen YB. In situ measurement of strong wind velocity spectra and wind characteristics at Keelung coastal area of Taiwan. Atmos Res 2001;57(3):171–85.
- [54] Simiu E. Wind spectra and dynamic alongwind response. Journal of the structural division. 1974;100(Proc. Paper 10815).
- [55] LeCun Y, Boser B, Denker JS, Henderson D, Howard RE, Hubbard W, et al. Backpropagation applied to handwritten zip code recognition. Neural Comput 1989;1(4):541–51
- [56] Krizhevsky A. In: Hinton H (editor). GE: Imagenet classification with deep CNN. Adv Neural Inform Process Syst. 2012;1097–105.
- [57] Maturana D, Scherer S. Voxnet: A 3d convolutional neural network for real-time object recognition. In: 2015 IEEE/RSJ International Conference on Intelligent Robots and Systems (IROS), IEEE, 2015, September, p. 922–8.
- [58] Kheradpisheh SR, Ganjtabesh M, Thorpe SJ, Masquelier T. STDP-based spiking deep convolutional neural networks for object recognition. Neural Netw 2018;99: 56–67.
- [59] Xiang Z, Rashidi A, Ou G. An Improved Convolutional Neural Network System for Automatically Detecting Rebar in GPR Data. 2019. arXiv preprint arXiv: 1007.0007.
- [60] Zhou L, Gu X. Embedding topological features into convolutional neural network salient object detection. Neural Netw 2020;121:308–18.
- [61] Karimi S, Dai X, Hassanzadeh H, Nguyen A. Automatic diagnosis coding of radiology reports: a comparison of deep learning and conventional classification methods. In: BioNLP 2017, 2017, August. p. 328–32.
- [62] Zhang YD, Dong Z, Chen X, Jia W, Du S, Muhammad K, et al. Image based fruit category classification by 13-layer deep convolutional neural network and data augmentation. Multimedia Tools Appl 2019;78(3):3613–32.
- [63] Avci O, Abdeljaber O, Kiranyaz S, Inman D. Structural damage detection in real time: implementation of 1D convolutional neural networks for SHM applications. In: Structural Health Monitoring & Damage Detection, Springer, Cham, 2017, Vol. 7, p. 49–54.
- [64] Gulgec NS, Takáč M, Pakzad SN. Structural damage detection using convolutional neural networks. In: Model validation and uncertainty quantification, 2017, Vol. 3, p. 331–7. Springer, Cham.
- [65] Maeda H, Sekimoto Y, Seto T, Kashiyama T, Omata H. Road damage detection using deep neural networks with images captured through a smartphone. 2018. arXiv preprint arXiv:1801.09454.
- [66] Lee K, Byun N. A Damage Localization Approach for Rahmen Bridge Based on Convolutional Neural Network. KSCE J Civ Eng 2020;24(1):1–9.
- [67] Zhang L, Yang F, Zhang YD, Zhu YJ. Road crack detection using deep convolutional neural network. In: 2016 IEEE international conference on image processing (ICIP), 2016, September, p. 3708–12. IEEE.
- [68] Cha YJ, Choi W, Büyüköztürk O. Deep learning-based crack damage detection using convolutional neural networks. Comput-Aided Civ Infrastruct Eng 2017;32 (5):361–78.

- [69] Dorafshan S, Thomas RJ, Maguire M. Comparison of deep convolutional neural networks and edge detectors for image-based crack detection in concrete. Constr Build Mater. 2018;186:1031–45.
- [70] Fan Z, Wu Y, Lu J, Li W. Automatic pavement crack detection based on structured prediction with the convolutional neural network. 2018. arXiv preprint arXiv: 1802.02208.
- [71] ASCE. Guidelines for Electrical Transmission Line Structural Loading. Reston: American Society of Civil Engineering. 3rd ed. ASCE: Virginia; 2010.
- [72] Davenport AG. The spectrum of horizontal gustiness near the ground in high winds. Q J R Meteorolog Soc 1961;87(372):194–211.
- [73] Tort C, Şahin S, Hasançebi O. Optimum design of steel lattice transmission line towers using simulated annealing and PLS-TOWER. Comput Struct 2017:75–94.
- [74] Fu X, Li HN, Wang J. Failure analysis of a transmission tower subjected to combined wind and rainfall excitations. Struct Des Tall Spec Build 2019;28(10): e1615.
- [75] Gupta S, Zhang, W, Wang, F. Model accuracy and runtime tradeoff in distributed deep learning: A systematic study. In: 2016 IEEE 16th International Conference on Data Mining (ICDM), 2016, December. p. 171–80. IEEE.
- [76] He K, Sun J. Convolutional neural networks at constrained time cost. In: Proceedings of the IEEE conference on computer vision and pattern recognition; 2015. p. 5353–60.
- [77] Urban G, Tripathi P, Alkayali T, Mittal M, Jalali F, Karnes W, et al. Deep learning localizes and identifies polyps in real time with 96% accuracy in screening colonoscopy. Gastroenterology 2018;155(4):1069–78.
- [78] Uchida S, Ide S, Iwana BK, Zhu A. A further step to perfect accuracy by training cnn with larger data. In: 2016 15th International Conference on Frontiers in Handwriting Recognition (ICFHR), 2016, October, p. 405–10. IEEE.
- [79] Cho J, Lee K, Shin E, Choy G, Do S. How much data is needed to train a medical image deep learning system to achieve necessary high accuracy? 2015. arXiv preprint arXiv:1511.06348.
- [80] Zabidi A, Yassin IM, Hassan HA, Ismail N, Hamzah MMAM, Rizman ZI, et al. Detection of asphyxia in infants using deep learning convolutional neural network (CNN) trained on Mel frequency cepstrum coefficient (MFCC) features extracted from cry sounds. J Fundament Appl Sci 2017;9(3S):768–78.
- [81] Al-Ajlan A, El Allali A. CNN-MGP: Convolutional neural networks for metagenomics gene prediction. Interdisc Sci: Comput Life Sci 2019;11(4):628–35.
- [82] Cui Z, Yang J, Qiao Y. Brain MRI segmentation with patch-based CNN approach. In: 2016 35th Chinese Control Conference (CCC), 2016, July. p. 7026–31. IEEE.
- [83] Simiu E, Scanlan RH. Wind effects on structures: fundamentals and applications to design. 1996.
- [84] ASCE. WIND LOADS ON BUILDINGS—MWFRS (DIRECTIONAL PROCEDURE). In: Minimum Design Loads for Buildings and Other Structures. Reston, Virginia: American Society of Civil Engineers/Structural Engineering Institute; 2006.